UNIVERSITÀ
DEGLI STUDI
DI TORINO

Doctoral Dissertation

Doctoral Program in
Bioengineering and Medical-Surgical Sciences (32nd Cycle)

Development of Computational Multibody Models of Anatomical and Prosthetic Knee Joints as Evaluation Tool for Orthopaedic Interventions and Prosthesis Design

Giovanni Putame

* * * * * *

Supervisor
Prof. Alberto Audenino

Doctoral Examination Committee:
Prof. Rainer Bader, Referee, University of Rostock
Prof. Andrea Corvi, Referee, University of Florence

Politecnico di Torino 2020

I hereby declare that, the contents and organisation of this dissertation constitute my own original work and does not compromise in any way the rights of third parties, including those relating to the security of personal data.

Giovanni Putame

Abstract

The knee represents one of the most complex joint of the musculoskeletal apparatus being characterized by a three-dimensional kinematics which results from the concurrence of translational and rotational motions among the articulating bones forming the joint. The complexity of the knee kinematics derives by the interaction of different anatomical structures. Especially, ligaments play a critical role in defining the range of motion of the knee, since they represent the major articular restraining elements. An alteration of the balancing among the constraining actions exerted by the ligaments, together with the other soft tissue surrounding the joint, leads to modifications in the joint kinematics and, consequently, to the establishment of detrimental intra-articular loading conditions. In fact, ligaments deficiency can result in serious degenerative knee injuries (e.g., osteoarthritis and joint wear). Furthermore, the knee is particularly vulnerable to acute trauma and to the development of arthritis and osteoporosis that are among the main causes for disability and pain in the modern society. Issues related to the

knee functionality are relevant for both humans and dogs, indeed, since the joint anatomy and kinematics are comparable between the two species, they shear similar knee injuries as well as relative surgical treatments. In order to alleviate pain caused by pathological conditions and to restore the functionality of the knee joint, when the non-surgical treatments fail, different orthopaedic surgical approaches can be pursued, for instance, corrective osteotomies and prosthesis implantation. Focusing on arthroplasty, a successful surgical outcome depends on various technical factors including accurate bone resection, proper prosthesis positioning, and adequate soft tissue balancing. In the last years, the introduction of even more sophisticated mechanical tools and computer-assisted surgical systems has made it possible to improve the accuracy of the procedures and, thus, enhance surgical outcomes. Nevertheless, essential information, such as intra-articular contact pressure and soft tissues tensioning, remain still challenging or even impossible to measure during a surgical intervention in an operative room.

In this context, the integration of computational simulations into the surgical decision-making process appears as an appealing solution to address this lack of information and to quantify surgical parameters that, usually, are just qualitatively evaluated. In particular, the multibody modelling of joints has been proven to be an effective approach to estimate significative quantities, such as forces related to ligaments, tendons, muscles, and intra-articular contacts, in addition to relative motions between bones. Especially, the development of even more accurate patient-specific biomechanical models, coupled with surgical navigation

systems and specifically designed sensing devices, could lead to a better understanding of the joint biomechanics as well as to the implementation of valuable tools aimed at supporting surgeons throughout the pre-, intra- and post-operative phases, providing additional data to foresee consequences of surgical interventions and also improve actual surgical techniques.

In this thesis work, various modelling strategies have been properly exploited to investigate specific orthopaedic issues related to the biomechanical behaviour of the anatomical and artificial knee joint in canine and human subjects, respectively. In detail, three distinct multibody models have been created in order to (1) compare the effectiveness of two alternative osteotomies in treating the anterior cruciate ligament rupture in dogs, (2) interactively investigate the impact of different knee implant configurations on the collateral ligaments tensioning after total knee arthroplasty (TKA) in humans, and (3) compare the performance of two different implant designs for TKA in humans. Overall, the implemented multibody models allowed to obtain realistic kinematics and dynamics results, including ligament tensioning and intra-articular contact force.

Findings of this work would contribute to confirm the feasibility of applying the multibody approach to obtain significative information for improving orthopaedics surgical outcomes, especially, those related to knee arthroplasty. Furthermore, multibody simulations manage to provide a realistic investigation of knee implants performance, which is essential for the implant design developments and optimizations.

Acknowledgment

I wish mainly to thank my supervisor, Professor Alberto Audenino, who left me free to follow my interests and to express myself in my research activities. I am also deeply grateful to Dr. Mara Terzini and Dr. Diana Massai who counselled me along my PhD path. I would like also to thank Professor Rainer Bader and Märuan Kebbach, who welcomed me in Rostock and introduced me to the beauty of the Baltic sea.

I would like to thank my family, which always trusted me and, with brave altruism, let me move far from home. A special thanks goes to my partner, Roberta, who believes in me, encourages my work, relieves my concerns making me smile as no one else, and, just sometimes, also stands me.

Last, but not least, I wish to thank all colleagues (let me say friends) of mine, who are able to turn a working place into a place where to have fun, often together with lots of food, and where to receive support during the inevitable hard times.

Heartfelt thanks to all of you

I would like to dedicate
this thesis to my family

Contents

List of Tables

List of Figures

Chapter 1

Introduction

This first chapter is intended to give a general overview on the multibody modelling approach and, especially, its application into the orthopaedic surgery field. Moreover, the structural anatomy of the canine and human knee joint is illustrated. Finally, the goals and outline of the present work are delineated.

1.1 Multibody simulation in orthopaedics

Nowadays, computational methods are widely used in biomechanical studies. Essentially, finite-element analyses (FEA) and multibody analyses represent the two mostly used computational approaches to address musculoskeletal research topics. Based on concepts related to the continuum mechanics, FEA aim mainly at predicting stress and strain distributions within hard and soft biological tissues. However, due to its high computational costs, FEA are generally applied to small-scale

systems involving static loading conditions. On the other hand, based on the dynamic equations of motion, multibody analyses allow to investigate kinematics and dynamics behaviours of systems, which are consisting, basically, of multiple rigid or flexible bodies interconnected by joints. In contrast to FEA, traditional multibody analyses are not able to give information about stress or strain distributions but offer the possibility to deal with small- as well as large-scale systems even implying low computational costs. In this context, the musculoskeletal apparatus can be, partially or totally, modelled as a complex multibody system and different valuable quantities, such as forces related to ligaments, tendons, muscles, and articular contacts, in addition to translations and rotations of the bone segments, can be rapidly obtained as simulations outcomes.

In light of the above-mentioned advantages, multibody simulations appear particularly suitable for clinical applications, especially those related to the orthopaedic field. In general, among the earliest applications of multibody approach there is the study of the human locomotion in 1906 (Schiehlen, 1997). Since then, multibody simulations gained even more popularity in biomechanics. Also, the implementation of new specifically built software, for example, Anybody (AnyBody Technology, Aalborg, Denmark) and OpenSim (open-source software, available from https://opensim.stanford.edu/), made multibody modelling more accessible, furtherly increasing its diffusion. In this thesis, all presented multibody models were created in ADAMS View (MSC Software Corporation, Santa Ana, CA), that is, a general-purpose multibody software. Such choice

allowed for a full control on the created model at expense of a greater initial effort in developing each modelling element.

In the body of literature, numerous different applications of the multibody approach in biomechanics can be found, such as: to develop and assess the performance of prosthetic devices (Grosu et al., 2014; Müller et al., 2016; Pascoletti et al., 2018); to predict articular contact forces in human and animal joints (Chen et al., 2014; Fregly et al., 2012; Harrison et al., 2010; Hu et al., 2018); to investigate the effect of ligament deficiency on joint kinematics and dynamics (Guess and Razu, 2017; Kang et al., 2017; Rahman et al., 2018), to evaluate athletes performance during sport activities (Mahadas et al., 2019), to understand typical and impaired neuromuscular control (Seth et al., 2018), etc.

Focusing on arthroplasty, multibody models of anatomical structures aim at supporting surgeons throughout the pre-, intra- and post-operative phases providing additional information useful to improve surgical outcomes. Reported studies referring to the pre-operative phase have the primary purpose to foresee consequences of surgical interventions. More in detail, these studies aim at predicting how the surgical variables will affect the post-operative kinematics, soft tissues functionality (e.g. ligament tension/strain, muscle strengths, cartilage compressions) or intra-articular contact forces. For instance, by means of a patient-specific model, Viceconti and collegues (2019) performed a pre-operative prediction of the knee ligament elongations, during level walking, due to total knee arthroplasty as a function of position and orientation of the knee implant. Moreover, Geier et

al. (2017) carried out a systematic analysis, using a lower limb model integrated into a hardware-in-the-loop simulation, to study the impact of implant position, design, and impaired muscle function, on total hip implant dislocation. Other parametric studies confirmed the efficiency of the multibody approach in predicting the range of motion of a prosthetic joint in relation to its components positioning (Morra et al., 2008; Pianigiani et al., 2012; Putame et al., 2019).

Moreover, the analysis of post-operative data could help to correlate surgical choices with relative outcomes, thus improving the actual surgical techniques. In this context, multibody simulations allow to estimate significant quantities that usually are difficult to obtain experimentally, such as the ligament elongation patterns (Hosseini Nasab et al. 2019), tibiofemoral contact forces (Navacchia et al. 2016), and accurate joint kinematics (Twiggs et al., 2018).

In the last years, the combination between patient-specific virtual models with surgical navigation systems has made it possible to accomplish very accurate spatial measurements during the intra-operative phase (e.g. relative positions and orientations between body segments and implant components). Nevertheless, significant quantities, such as intra-articular contact pressure and soft tissues tensioning, are still very challenging or even impossible to measure, except through expensive and/or highly invasive sensing devices. Intra-operative computational analyses could potentially provide such missing information as long as two main requirements are met: (1) compatibility of simulation time with the tight timing of surgical procedures; (2) integration of

patient-specific anatomical geometries as well as tissues mechanical properties into the model. Although the increasingly computational power and the continuous advancements of research, to date, only few studies tried to bring biomechanical simulations directly into the operating theatre. Among these studies, Armand et al. (2018) presented a simulation-based guidance system for periacetabular osteotomy which aims, by using a discrete element analysis, to provide joint contact pressures during the surgical intervention.

Overall, further efforts are necessary in order to make computational models even more reliable, thereby, increasing their adoption by surgeons. As future prospective, desirable outcomes could result from the combination of increasingly sophisticated sensing devices with more functionally accurate multibody models.

1.2 Knee anatomy in humans and dogs

The structural anatomy of the knee joint, also called stifle joint in quadrupeds, is very similar between humans and dogs. The knee represents the largest diarthrosis (i.e., synovial joint) of the body, consisting of two joints, namely, the patellofemoral joint and the tibiofemoral one, whose primary function is to connect the thigh with the leg permitting their flexion/extension relative movement as well as a minor internal/external rotation (Blackburn and Craig, 1980). The tibiofemoral joint articulates the medial and lateral femoral condyles, that is the distal end of the femur, with the corresponding condyles that form the

characteristic plateau of the proximal tibia. In details, the medial femoral condyle is larger than the lateral one, and both can be approximated by ellipsoidal shapes (Goldblatt and Richmond, 2003). The patellofemoral joint articulates the patella with the femoral trochlea. During the knee flexion and extension, the patella slides into the trochlear groove increasing the knee stability and, acting as a pulley, allowing an effective transfer of the muscle action force across the joint.

Bony segments are connected by the articular ligaments, namely, biological tough fibrous bands, forming the articular joint. Ligaments act as the main passive constrain that give stability and define the range of motion of a joint. Briefly, a ligament is composed of dense connective tissue including cells (i.e., fibroblasts) and extracellular matrix which, in turn, is mainly composed by type I collagen fibrils together with a small amount of proteoglycan, elastin, and other proteins (Nordin and Frankel, 2012). Collagen fibrils aggregate in the extracellular matrix in a parallel arrangement to form fibers which aggregate further into bundles. These collagenous fibers results in line with the axis of the ligament and constitute the structure that bear the tensile load to which the ligaments are subjected during the joint movement. For the sake of brevity, just the major ligaments of the knee here are described, these include: the medial and lateral collateral ligaments, the anterior and posterior cruciate ligaments, the medial and lateral patellofemoral ligaments, and the patellar ligament (Figure 1-4). The medial collateral ligament (MCL) appears as a broad and flat membranous band. It originates from the medial epicondyle of the femur and inserts on the medial

proximal body of the tibial bony segment. The anterior bundle progressively tightens over the knee flexion, while the posterior bundle slackens. The lateral collateral ligament (LCL) appears thinner than the MCL. It arises from the lateral epicondyle of the femur, then it finds its insertion on the head of the fibula below. The stretching behaviour of its anterior and posterior bundle is comparable to that of the MCL. Cruciate ligaments mainly guaranty the knee joint stability on the sagittal plane (Kweon et al., 2013). Both ligaments consist of two distinct bundles. In particular, the anterior cruciate ligament (ACL) is attached between the posteromedial surface of the lateral femoral condyle and the area anterior to and between the intercondylar eminences of the tibial plateau. Its anteromedial bundle (aMCL) is taut in flexion, while the posterolateral bundle (pACL) results taut in extension. The posterior cruciate ligament (PCL) is arranged almost symmetrically with respect to the ACL. It connects the lateral surface of the medial femoral condyle to a central area located posteriorly and inferiorly to the tibial plateau. Its anterolateral bundle is lax in extension, becoming taut in flexion, conversely the posteromedial bundle is stretched in extension and lax in flexion. The medial (mPFL) and lateral (lPFL) patellofemoral ligaments are the main stabilizer of the patella against mediolateral dislocations. They originate from the superior lateral and medial aspect of the patella and inserts in the space between the adductor tubercle and the femoral epicondyle on the relative side.

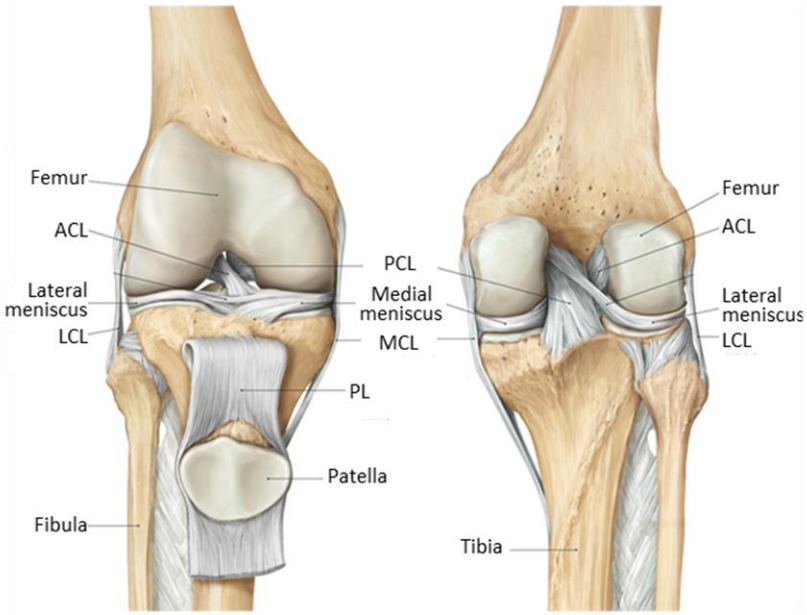

Figure 1. Bones and main ligaments of a right human knee. Frontal (left) and posterior (right) view. ACL: anterior cruciate ligament; PCL: posterior cruciate ligament; MCL: medial collateral ligament; LCL lateral collateral ligament. PL: patellar ligament. Adapted from Schünke et al. (2014)

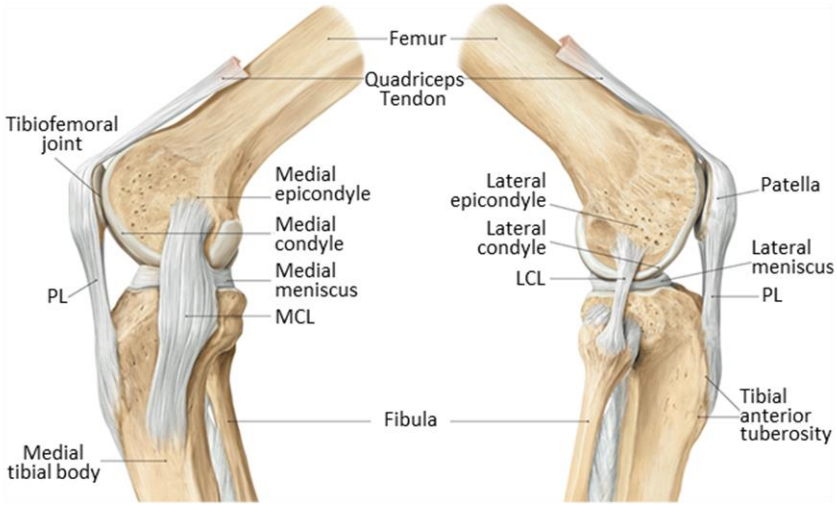

Figure 2. Bones and main ligaments of a right human knee. Medial (left) and lateral (right) view. MCL: medial collateral ligament; LCL lateral collateral ligament. PL: patellar ligament. Adapted from Schünke et al. (2014)

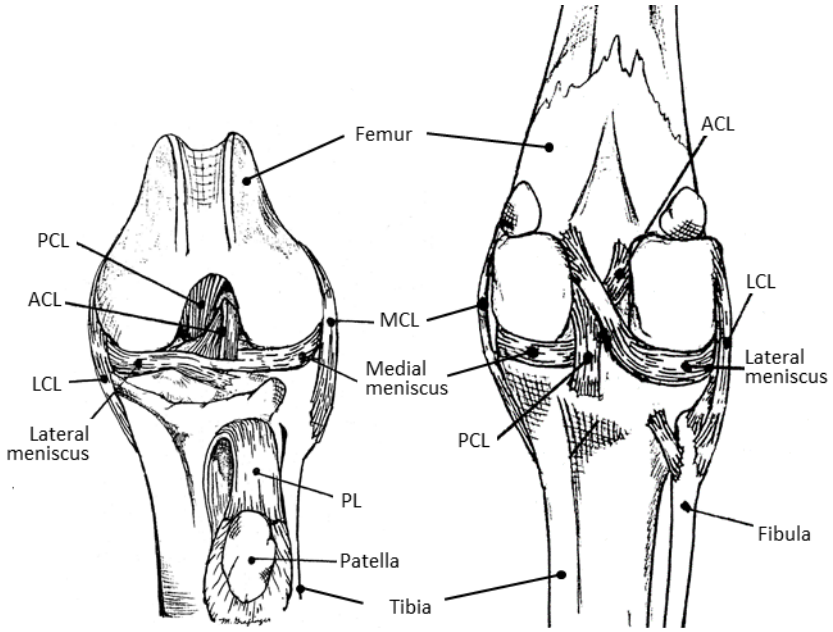

Figure 3. Bones and main ligaments of a right canine knee. Frontal view at flexion (left) and posterior (right) view at extension. ACL: anterior cruciate ligament; PCL: posterior cruciate ligament; MCL: medial collateral ligament; LCL lateral collateral ligament. PL: patellar ligament. Adapted from Carpenter and Cooper (2000)

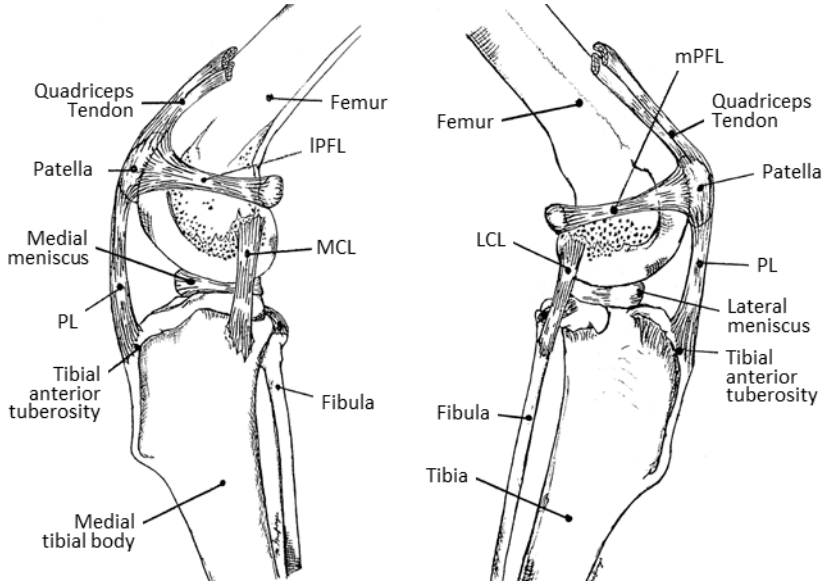

Figure 4. Bones and main ligaments of a right canine knee. Medial (left) and lateral (right) view. lPFL: lateral patellofemoral ligament; mPFL: medial patellofemoral ligament; MCL: medial collateral ligament; LCL lateral collateral ligament. PL: patellar ligament. Adapted from Carpenter and Cooper (2000)

The patellar ligament (PL), often referred to as patellar tendon, plays a fundamental role in the extensor mechanism of the knee. It consists of a flat band which runs from the anterior tuberosity of the tibia up to the distal apex of the patella, then it extends over the patellar surface merging into the quadriceps tendon.

Besides ligaments, other important anatomical structure are the menisci. These consist in a couple of crescent-shaped fibrocartilaginous structures which help to increase the global joint stability. Moreover, the menisci allow to reduce the force concentration at the tibiofemoral interface by increasing the congruence between femoral and tibial condyles.

As regards muscles involved in the knee motion, the quadriceps femoris represents the primary extensor muscle group including vastus medialis, vastus intermedius, vastus lateralis and rectus femoris. Other muscle that deserve to be mentioned are the hamstrings muscle group, which act as quadriceps antagonist, and the muscles of the calf, among these the gastrocnemius is also involved in the knee flexion. In addition to the ligaments constraining action, muscles crossing the knee contribute to improve the joint stability.

Although showing different ranges of motion, the knee kinematics is essentially comparable between human and dogs (Richard et al., 2010). Indeed, the knee joint allows mainly for flexion/extension movements on the sagittal plane. For this reason, the knee joint is sometimes simplified as a hinge. However, in-depth kinematics analyses revealed the occurrence of specific secondary movements, such as a medial-pivoting

movement throughout the flexion range, that is, an internal/external tibial rotation around the medial condyle. In particular, a movement known as “screw-home mechanism” was also observed. Such mechanism implies an external tibial rotation over higher extension angles, leading to the ligaments tightening and, consequently, improving the joint stability in extension (H. Y. Kim et al., 2015).

In addition, it is well known that, due to a combination of rolling and sliding movements, a posterior translation of the femoral condyles occurs toward deeper flexion angles. All together, these movements make the knee joint kinematics one of the most complex in the whole musculoskeletal apparatus.

1.3 Aim of the work and outline

The overall aim of this thesis is to improve the understanding of specific orthopaedic issues involving the canine and human knee joint. In detail, three major objectives were established and addressed by means of a common multibody approach:

- To develop a canine knee model in order to virtually perform two alternative surgical procedures and compare their effectiveness in the treatment of the anterior cruciate ligament rupture
- To develop a human prosthetic knee model, equipped with an interactive software interface, able to give information on the ligament balancing during total knee arthroplasty

- To develop the multibody model of a human lower limb to investigate the biomechanical performance of two different insert designs for total knee arthroplasty, giving special attention to the tibiofemoral contact modelling in order to obtain contact locations and pressure distributions on the insert surface directly within the multibody framework

Overall, the present work is organized in three main parts. First, a general introduction on the multibody modelling approach and its application into the orthopaedic field is provided. Moreover, an overview about the structural anatomy of the canine and human knee joint is illustrated.

The second part focuses on the strategies employed for the creation of the presented biomechanical multibody models. In detail, the mathematical formulations behind the implementation of ligaments, menisci, contact mechanics and muscle action were presented.

In the third part, three specific case studies are reported, each including: the background information about the investigated topic, the detailed description of the created multibody model, and the obtained results with the relative discussion.

Finally, the main conclusions of the present work are offered.

Chapter 2

Modelling Strategies

In this chapter, the specific modelling approaches exploited throughout this work are presented. Any further detail will be specified in the dedicated “Model” section of each case study treated in the next chapter.

2.1 Ligaments

In the past decades, several research groups investigated the biomechanical behavior of ligaments in terms of stress and strain during specific articular movements. Indeed, different models were proposed to mathematically describe the force-strain relationship of ligaments under loading conditions. In general, ligaments are modelled by using line (1D), planar (2D) or solid (3D) elements (Galbusera et al., 2014). Although 2D and 3D elements potentially can offer additional information with respect

the 1D elements, such as ligaments local strains, these latter present some attractive advantages, that are, a straightforward numerical implementation and high computational efficiency.

In this thesis, based on the work purposes, the 1D approach has been chosen. One of the most used 1D ligament models was proposed by Blankevoort et al. in 1991. This model represents each ligament bundle as single tension-only spring element connecting the origin and insertion points. In particular, the force-strain relationship of each spring is described by the following nonlinear piecewise function:

$$f = \begin{cases} -k(\varepsilon - \varepsilon_L), & \varepsilon > 2\varepsilon_L \\ -0.25\, k \dfrac{\varepsilon^2}{\varepsilon_L}, & 0 \le \varepsilon \le 2\varepsilon_L \\ 0, & \varepsilon < 0 \end{cases} \quad (1)$$

where ε is the ligament strain, ε_L is a reference value of strain assumed to be 0.03 and k is the stiffness parameter, expressed as force per unit strain, of each different ligament bundle. The ligament strain ε is defined as:

$$\varepsilon = \frac{(l - l_0)}{l_0} \quad (2)$$

where l is the actual ligament length and l_0 is the zero-load length, also called slack length, that is, the maximum linear distance between the ligament attachment points above which the ligament gets taut. The force-strain curve obtained for a ligament modelled through the function proposed by Blankevoort et al.

(1991) is depicted in Figure 5. In detail, two regions can be identified, the toe region for lower strain ($\varepsilon < 2\varepsilon_L$), and the linear region for higher strain ($\varepsilon > 2\varepsilon_L$) where the ligament force is determined by the stiffness parameter (i.e., the slope of the straight line). In order to consider the different recruitments patterns of the fiber bundles within the same ligament, during the joint movement, each bundle is treated as a single parallel spring, thus, the total stiffness value is equally divided among the springs.

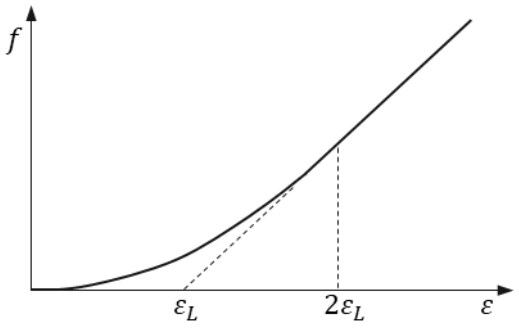

Figure 5. Force-strain curve obtained for a ligament modelled through the function proposed by Blankevoort et al. (1991). The strain value equal to $2\varepsilon_L$ defines the limit between the toe region ($\varepsilon < 2\varepsilon_L$) and the linear region ($\varepsilon > 2\varepsilon_L$).

Following the described constitutive model, the viscoelastic behavior of the ligaments is neglected. Nevertheless, in order to avoid high frequency vibrations during the multibody simulations, a parallel damper with a damping coefficient of 0.5 Ns/mm can be added to each spring element (Guess et al., 2010).

An important aspect, that deserves to be deepened, is the determination of the zero-load length l_0 for each considered

ligament bundle. Indeed, this parameter is closely related to the reference strain, that is, the strain of the ligaments at a given joint reference position, usually the full extension for the knee. The following expression relates the zero-load length l_0 with the reference strain ε_R:

$$l_0 = \frac{l_R}{\varepsilon_R + 1} \tag{3}$$

where l_R is the ligament length at the reference joint position. Unfortunately, reference strains are challenging to measure experimentally. Therefore, often they are adapted from previous experimental studies (Blankevoort, Kuiper et al., 1991; Trent et al., 1976; Wismans et al., 1980). In this work, starting from reported values, two different strategies were used to refine the zero-load lengths.

The first consists in the assessment of the joint behavior by simulating a laxity test. In this case, the joint is subjected to specific loading conditions (e.g., the clinical drawer test) and the related displacements are measured and compared with experimental data. Then, the zero-load lengths are refined until numerical results match the experimentally reported data.

The second is derived from the study of Guess and Razu (2017) which proposed a systematic strategy based on two assumptions: during the passive movement of the knee, throughout its range of motion, (1) every ligament bundle is stretched and (2) the force exerted by each bundle should be

below 50 N. An in-depth description about the zero-load lengths determination will be addressed later for each case study.

2.2 Menisci

In order to investigate the behavior of an anatomical joint, it is important to include all the significant constraining elements. From a modeling point of view, the implementation of an anatomical knee model is more challenging than a prosthetic one because of the presence of biological structures that are instead sacrificed during a common total knee arthroplasty. Indeed, depending on the knee prosthesis design, only the anterior or both anterior and posterior cruciate ligaments as well as the menisci and part of the articular capsule are resected.

In the anatomical knee, besides ligaments, the menisci contribute to improve the joint stability, especially, related to the femoral sliding on the tibial plateau.

In the multibody context, to our knowledge, three approach to model menisci were proposed. The first, introduced by Lu and co-workers (Li et al., 1999), emulates only the constraining forces due to the menisci. Therefore, details of the meniscal geometry were neglected as well as femoro-meniscal and tibio-meniscal contact forces. Each meniscus (medial and lateral) is represented by two perpendicular springs, acting on the tibial plateau in the anteroposterior and mediolateral directions, respectively. Moreover, each spring is constrained at one end on the tibial plateau and at the other end to the femoral condyle. Such approach can be easily implemented by using a simplified

formulation of the bushing element* considering the effect of only two translational forces as represented below:

$$\begin{bmatrix} F_x \\ F_y \\ F_z \end{bmatrix} = \begin{bmatrix} K_{11} & 0 & 0 \\ 0 & K_{22} & 0 \\ 0 & 0 & 0 \end{bmatrix} \cdot \begin{bmatrix} x \\ y \\ z \end{bmatrix} \quad (4)$$

where F_x and F_y are the meniscal constraining forces in the anteroposterior and mediolateral direction, respectively. The force F_z normal to the tibial plateau is null. The K_{ij} coefficients represent the stiffness values. Finally, x, y and z are the translations along the respective perpendicular directions.

A second approach takes into account the geometry of each meniscus as a single rigid body connected to the tibial plateau (Hu et al., 2018). Therefore, two additional meniscus-cartilage contacts pairs are included into the model and the respective forces can be obtained.

The last approach, presented by Guess et al. (2010), implies the discretization of each meniscus in elements connected through a bushing element defined by a 6×6 stiffness matrices. Intuitively, since this approach makes the model more complex to solve, it should be considered only when the aim of the study is the investigation of the meniscal behavior. In this thesis, the first above-mentioned approach was used.

* The bushing element allows to generate a six-components force (3 translational forces and 3 torques) acting between two bodies depending on their relative linear and angular displacements and velocities. Thus, in general, the bushing element is defined by a 6x6 stiffness matrix and a 6x6 damping matrix.

2.3 Contacts

Generally, biomechanical models involve idealized joints (e.g., spherical, revolute, universal) in order to represent the principal degrees of freedom (DOF) of the considered anatomical joint. For instance, the arthrodial joint of the elbow is often idealized as a simple revolute joint. However, to better investigate intra-articular contact forces and the real kinematic of anatomical or prosthetic joints, the constraining forces due to biological soft tissues (e.g., ligaments, tendons, menisci) must be taken into account, in addition to the geometry of the articulating surfaces and their material properties. The selection of a proper contact representation for the simulation of biomechanical multibody systems is very important to reduce the generation of high-frequency vibrations into the system, which negatively affects the required computational times. In this work, two most common formulations were used to include compliant contacts into the presented multibody models, both characterized by advantages and disadvantages (Flores et al., 2016; Sherman et al., 2011). The first is described by an interpenetration formulation derived from the Hertz's contact theory, the second is based on the elastic foundation theory. Both strategies are modified to include energy dissipation phenomena (Flores, 2011). In addition, the contribution of the friction force, when considered, was computed by using a Coulomb's model and added to the contact force.

2.3.1 Hertz's law-based formulation

The Hertz's law-based formulation, used in this work, is derived from that proposed by Hunt and Crossley (1975). The contact force F_c is calculated based on both penetration depth between the undeformed contacting bodies and penetration velocity as follows:

$$F_c = K\delta^e + C(\delta, \delta_{max}, C_{max})\dot{\delta} \tag{5}$$

where K is the contact stiffness constant, δ is the penetration depth (Figure 6), e is the nonlinear power exponent, $\dot{\delta}$ is the penetration velocity and C is a sigmoid damping function which depends on the penetration depth and it is defined by a maximum penetration constant δ_{max} at which the damping function reaches its maximum value C_{max}. On the right side of the equation, the first term is the elastic force component while the second term represents the energy loss during the contact. In order to avoid discontinuities at the initial instant of contact, unlike what reported by Hunt and Crossley, the second term is multiplied by a sigmoid function that is proportional to the penetration. Finally, the single vector force F_c is applied at the centroid of the interpenetration volume. Although this formulation is numerically efficient, the determination of the associated stiffness and damping parameters is difficult due to the lack of experimental data.

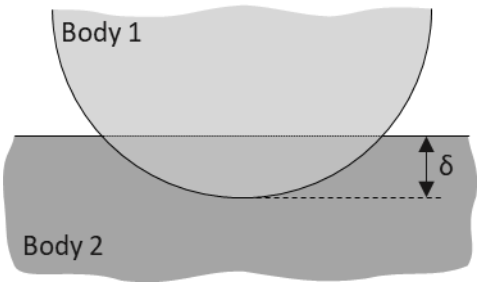

Figure 6. Schematic representation of the Hertz's law-based contact between two rigid bodies. The distance δ is the penetration depth.

2.3.2 Elastic foundation theory-based formulation

The alternative approach here considered for the prediction of the contact force is based on the elastic foundation theory, hence it involves the creation of a layer of independent elastic elements which covers the contact surface of the deformable body. Specifically, in the present work, this approach was applied to investigate the contact forces that arise at the interface between the metal femoral component and the plastic tibial insert of a total knee prosthesis. Considering the material properties of these contacting bodies, the femoral component was assumed as rigid, in contrast, the tibial insert undergoes small deformations, thus a linear formulation was considered suitable for our purpose. In particular, the pressure p acting on each elastic element can be expressed by the following formula:

$$p = \frac{(1-\nu)\,E\,\delta}{(1+\nu)(1-2\nu)\,h} \tag{6}$$

where E is Young's modulus of the deformable layer, v is Poisson's ratio of the layer, h is the layer thickness, and δ is the spring deformation, that is, the interpenetration between the contacting bodies (Figure 7).

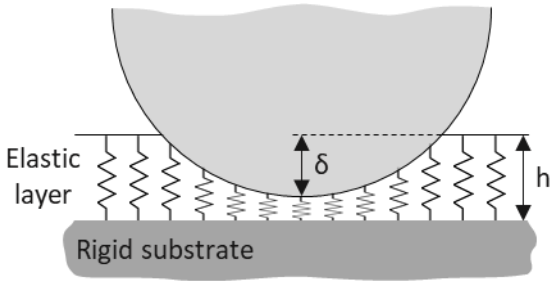

Figure 7. Schematic representation of the elastic foundation theory-based contact where h is the layer thickness, and δ is the spring deformation.

Since this approach is not implemented by default in the used software ADAMS, a macro code was specifically created in order to automatically discretize a rigid body, that is, in our case, the tibial insert of the knee prosthesis. In detail, the implemented macro allows to, firstly, discretize the tibial insert into hexahedral elements with a specified cross-sectional area, successively, the base of each discretized element is rigidly connected on the upper surface of the tibial tray of the knee implant. Finally, a contact is defined between each element and the femoral component. The contact is defined using the Equation 5 considering the nonlinear power exponent as unitary (e = 1) and the stiffness constant K derived from the Equation 6, multiplying the ratio p/δ by the cross-section area of the discretized element. Moreover, in order to properly display the obtained contact pressure distribution

maps, a custom script was implemented in Matlab (MathWorks, Natick, MA).

The major advantage of this approach consists in the possibility to derive the contact stiffness as well as to obtain directly the contact pressure distribution within the multibody framework. Furthermore, it allows for an easier identification of the contact area location and extension.

2.3.3 DOE for contact parameters estimation

Since contact parameters are usually unknowns, the design of experiment (DOE) was adopted to estimate them with the objective to minimize the presence of high-frequency oscillations in the monitored contact force of interest, that is, the tibiofemoral contact force. Therefore, the contact stiffness, damping, and power exponent were all considered as design variables except for the case when the stiffness constant was derived by the elastic foundation theory. In order to start a DOE, a list of values for the design variables needs to be specified as well as an output to measure the simulation performance. In detail, initially the minimum contact stiffness was defined approximatively as the ratio between the expected contact force (Mizu-uchi et al., 2015) and the maximum allowed interpenetration depth. Then, this minimum estimated stiffness is used to compute the contact critical damping by means of the following formula derived from the mass-spring-damper model:

$$C_{cr} = 2\sqrt{K_e\, m} \tag{7}$$

where C_{cr} is the critical damping, K_e is the estimated stiffness and m is the mass of a contacting body with the other one fixed in space. Moreover, a value between 1 and 3 was assumed for the nonlinear power exponent (Müller et al., 2016). Once the initial values for the variables were roughly estimated, such values were divided and multiplied to define a reasonable range of discrete values (levels) for each variable. All possible variables combinations were investigated. As regarding the objective assessment, the power spectral density (PSD) of the tibiofemoral contact force was computed after each simulation, then the sum of the frequency contributions between 5 Hz and 50 Hz (limited range of unwanted frequency components) was taken as objective value to minimize, hence, the variables combination which generated the lowest objective value was selected. This approach is based on the assumption that the chosen variables levels do not significantly affect the simulation results except for the presence of high-frequency oscillations in the dynamics of the simulated model.

2.4 Muscles

In musculoskeletal modeling, muscles can be considered as actuators that, applying a traction force, move the articulated bony segments. Muscles are often represented using vector forces connecting, directly or through via-points, origin and insertion sites. In the context of this work, a closed-loop control algorithm (Figure 8) was implemented and integrated into some of the presented multibody models to estimate the muscle forces of interest needed in order to mimic a weight-bearing squat

movement. Such control algorithm is based on a proportional-integral-derivative (PID) controller (Fitzpatrick et al., 2012; Guess et al., 2014; Rahman, Sharifi Renani et al., 2018; Stylianou et al., 2013).

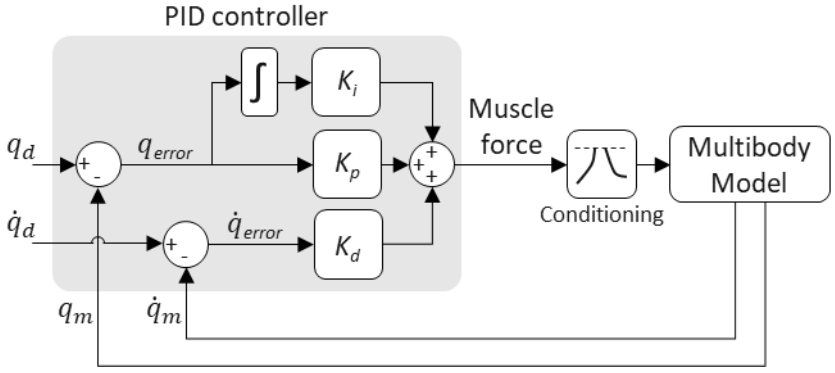

Figure 8. Control algorithm used to estimate the muscle force.

In detail, a reference spatial coordinate q_m and its derivative $\dot{q}_m$ (Figure 8, Figure 9a) are measured at each time-step of the model simulation, then, they are compared with desired values q_d and $\dot{q}_d$, respectively. Specifically, q_m and $\dot{q}_m$ represent, respectively, the actual position and velocity of the femoral head along the vertical direction y (Figure 9a), while q_d and $\dot{q}_d$ are defined by smooth time-dependent functions (5^{th} order polynomial having continuous first and second derivatives, Figure 10) that prescribe, respectively, the desired position and velocity of the femoral head during the knee flexion range. In the PID controller framework, the measured coordinate represents the input value, while the desired coordinate value represents the so-called setpoint value.

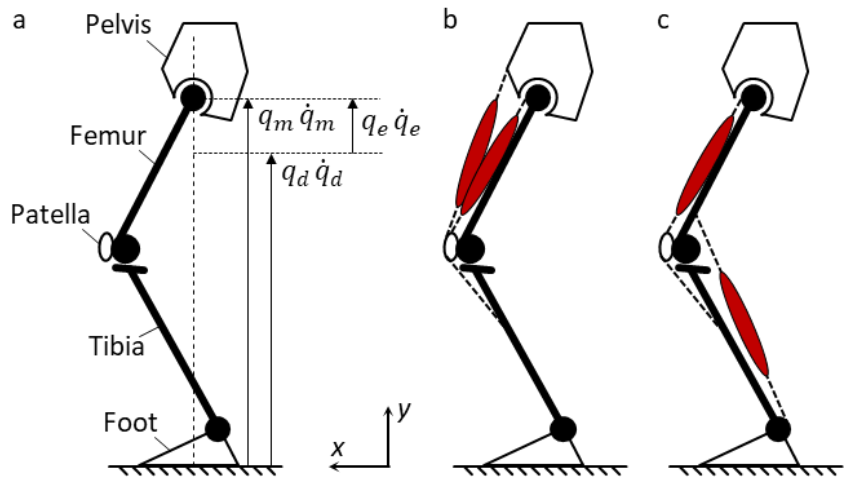

Figure 9. Explanatory 2D diagram of a lower limb on the sagittal plane. (**a**) measured coordinates ($\boldsymbol{q_m}$, $\boldsymbol{\dot{q}_m}$), desired coordinate values ($\boldsymbol{q_d}$, $\boldsymbol{\dot{q}_d}$) and relative errors ($\boldsymbol{q_e}$, $\boldsymbol{\dot{q}_e}$); (**b**) Model configuration presenting a muscle group (i.e. quadriceps); (**c**) Model configuration presenting two different unitary muscles (i.e. quadriceps and gastrocnemius).

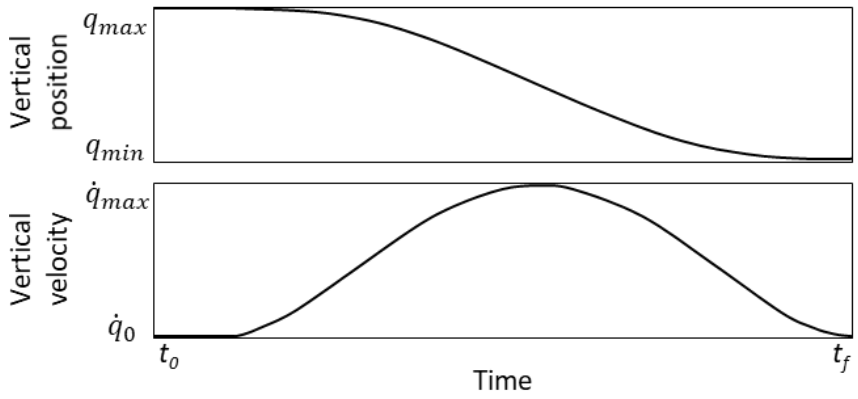

Figure 10. Explanatory charts showing the smooth time-dependent functions (5th order polynomial having continuous first and second derivatives) used to prescribe the desired vertical position (top) and the consequent velocity (bottom) of the femoral hip. The vertical position is defined between a maximum ($\boldsymbol{q_{max}}$) and a minimum ($\boldsymbol{q_{min}}$) limit, while the velocity ranges between zero ($\boldsymbol{\dot{q}_0}$) and a maximum value ($\boldsymbol{\dot{q}_{max}}$) reached at the middle of the motion duration (from $\boldsymbol{t_0}$ up to $\boldsymbol{t_f}$).

The setpoint values changes over time (Figure 10). Therefore, the PID controller continuously calculates the errors q_e and $\dot{q}_e$ as the difference between the measured and setpoint values, hence, it applies a correction aimed at minimizing the errors over time by adjustments of its output, which represents the generated muscle force.

In addition, the muscle force is conditioned so that only a traction force within a physiological range can be applied. In particular, an upper limit is estimated as the physiologic cross-sectional areas (PCSA) of the muscle multiply by a maximum isometric muscle stress equal to 1 MPa (An et al., 1989). A lower limit is also defined as 1% of the maximum force value (Shelburne and Pandy, 2002). This minimum constant force serves as preload to compensate tendon slack when these are included into the model. The force derived by the PID formulation is reported below:

$$f_{PID}(t) = K_p\, q_e(t) + K_i \int_0^t q_e(\tau)\, d\tau + K_d\, \dot{q}_e(t) \qquad (8)$$

where $f_{PID}(t)$ is the PID output, $q_e(t)$ is the position error, $\dot{q}_e(t)$ is the velocity error, and K_p , K_i , K_d are the proportional, integral and derivative gain, respectively.

In order to achieve the best performance, the *K* gains needs to be tuned. For the simplest limb models, where tendons are not modeled and articular surfaces are simplified, the Ziegler-Nichols tuning method, also called continuous cycling method, was chosen to refine the *K* gains (Ziegler and Nichols, 1993). This method requires to set the integral and derivative gains to zero.

Then, the proportional gain is increased from zero until it reaches the ultimate gain K_U at which the controller shows stable oscillations. The ultimate gain K_U and the measured oscillation period P_U are used to set the K_p, K_i and K_d gains by multiplying for predefined constants. In details, $K_p = 0.2 \cdot K_U$, $K_i = 0.2 \cdot K_U \cdot (2/P_U)$, $K_d = 0.2 \cdot K_U \cdot (P_U/3)$.

For the more complex models, for instance, with tendons and multiple muscle forces, a trial and error method were performed starting from reported values (Guess et al., 2014). In this case, K_p was increased until a position error lower than 1%, with respect to the total imposed translation, was obtained. Successively, the K_d was computed as $K_d = K_p \cdot 10^{-3}$, whereas the K_i was maintained equal to 5.

Specifically, two modelling configurations of the lower limb including multiple muscle forces were considered here. One configuration involves the modelling of the only quadriceps muscle group (Figure 9b), that is the main extensor muscle of the knee, which consists of four distinct muscles. In this case, to take into account the different muscle contribution, the controller output force (f_{PID}) was multiplied by the specific PCSA of each muscle normalized by the mean PCSA. The other configuration (Figure 9c) involves the modelling of the quadriceps and gastrocnemius each as a single traction force. In this case, the controller output force (f_{PID}) represents the quadriceps force, and the gastrocnemius force is derived by means of a scaling factor computed as the ratio between the two muscle PCSAs with the assumption that both muscles are fully recruited.

It should be note that, although computationally efficient, the implemented muscle modelling strategy implies some simplifications. For instance, unlike a Hill-type muscle model, physiological parameters which affect the force generation, such as contraction velocity and actual muscle length, were not explicitly took into account. However, in a first instance, a such refined muscle modelling was assumed unnecessary for the purposes of this work.

Chapter 3

Case studies

In this section the modelling approaches described in the second chapter are applied to investigate specific biomechanical case studies.

Surgical treatments for canine anterior cruciate ligament rupture: assessing functional recovery through multibody comparative analysis*

Anterior cruciate ligament (ACL) deficiency can result in serious degenerative knee injuries. Although tibial plateau levelling osteotomy (TPLO) is a common method for the surgical treatment of ACL deficiency, alternative osteotomies such as a levelling osteotomy based on the center of rotation of angulation (CBLO) are described in the literature. However, whether a CBLO could represent a viable alternative to a TPLO remains to be established. The aim of this study is to compare TPLO and CBLO effectiveness in treating ACL rupture.

First, a computational multibody model of a physiological knee was created using three-dimensional surfaces of a medium-sized canine femur, tibia, fibula and patella. Articular contacts were modelled by means of the Hertz's law-based formulation, describing the contact force as function of the interpenetration between surfaces. Moreover, ligaments were represented by vector forces connecting origin and insertion points. The lengths of the ligaments at rest were optimized simulating the drawer test.

Secondly, starting from this optimized physiological model, an ACL insufficiency was reproduced by deactivating the ACL

*__Based on:__ Putame G, Terzini M, Bignardi C, Beale B, Hulse D, Zanetti E and Audenino A (2019) "Surgical Treatments for Canine Anterior Cruciate Ligament Rupture: Assessing Functional Recovery Through Multibody Comparative Analysis". *Front. Bioeng. Biotechnol.* 7:180. doi: 10.3389/fbioe.2019.00180

related forces. These two first models were validated on reported *in vivo* experimental data (Korvick et al., 1994; Lopez et al., 2003, 2004). Hence, the TPLO and CBLO surgical procedures were virtually performed on the pathological knee.

Finally, the drawer test and a weight-bearing squat movement were performed to compare the treatments' effectiveness in terms of tibial anteroposterior translation, patellar ligament force, intra-articular compressive force and quadriceps force. Results from drawer test simulations showed that ACL-deficiency causes an increase of the anterior tibial translation by up to 5.2 mm, while no remarkable differences between CBLO and TPLO were recorded. Overall, squat simulations have demonstrated that both treatments lead to an increase of all considered forces compared to the physiological model. Specifically, CBLO and TPLO produce an increase in compressive forces of 54% and 37%, respectively, at 90° flexion. However, TPLO produces higher compressive forces (up to 16%) with respect to CBLO for wider flexion angles ranging from 135° to 117°. Conversely, TPLO generates lower forces in patellar ligament and quadriceps muscle, compared to CBLO. In light of the higher intra-articular compressive force over the physiological walking range of flexion, which was observed to result from TPLO in the current study, the use of this technique should be carefully considered.

3.1.1 Background

The main function of the anterior cruciate ligament (ACL) consists in the stabilization of the knee joint by limiting the anterior translation of the proximal tibia with respect to the distal

femur. The ACL insufficiency is an important orthopedic issue which can occur after acute trauma or, more commonly, it can arise from chronic pathological biomechanical stress and constitutes one of the main causes of lameness in dogs (S. E. Kim et al., 2008; Raske et al., 2013; Wilke et al., 2005). Furthermore, in the long term, the resulting knee instability leads to progressive osteoarthritis and severe meniscal injuries (Beer et al., 2018; Boudrieau, 2009; Pozzi et al., 2006). From a biomechanical point of view, the intra-articular forces acting on the tibial plateau under weight-bearing conditions can be resolved into a compressive force, perpendicular to the plateau, and an anterior-posterior (AP) directed force (tangential force), parallel to the plateau (Slocum and Slocum, 1993). The latter force, not being counteracted by the ACL action, is at the origin of excessive anterior tibial translation (i.e. drawer sign) which is the clinical sign of an ACL-deficient knee. Traditional surgery aimed at restabilizing the joint through different approaches classified as intra- and extra-articular procedures. Intra-articular approaches aim at replacing the ACL in its anatomical position, whereas, extra-articular approaches try to reduce the knee instability by means of soft tissue transposition or by using periarticular wires (S. E. Kim et al., 2008). Although these traditional approaches are widely used, they produce variable outcomes, especially in the long term. In this context, other surgical techniques based on tibial osteotomies have been developed with the aim of recreating the dynamic stability of the ACL-deficient knee. These techniques are based on a reduction of the tibial plateau slope in order to nullify the tangential articular force, which is responsible

for the out-of-range anterior tibial translation during weight bearing. Over the past decades, several tibial plateau leveling methods have been developed (Hildreth et al., 2006). Although most of these methods lead to positive clinical results, to date, the most effective surgical treatment based on tibial osteotomy has not been clearly identified yet. A common method is represented by the TPLO, which was first described in 1993 (Slocum and Slocum, 1993). It consists of a radial osteotomy centered at the intercondylar tubercles of the proximal tibia. Subsequently, a rotation of the proximal segment with respect to the distal one is performed to achieve a post-operative tibial plateau angle (TPA) equal to 5°. Another more recent technique is the CBLO (Raske et al., 2013). According to this method, the radial osteotomy is centered over the CORA point, which is defined as the intersection between the proximal and the diaphyseal tibial axes. Successively, the rotation of the proximal tibial segment aims at aligning the above mentioned two axes, thus obtaining a post-operative TPA equal to about 10°. For both these techniques, an internal fixation plate combined with surgical bone screws are required to maintain the modified orientation of the proximal tibial segment (Boero Baroncelli et al., 2013). In this scenario, *in silico* modelling can support comparisons among surgical techniques. Specifically, multibody analysis represents an effective computational approach to predict the biomechanical behavior of articular joints in terms of, for instance, range of motion (Zanetti et al. 2018) as well as intra-articular loads (Renani et al., 2018). When these models include also soft tissue such as muscles and ligaments, both active and passive forces,

respectively, can be estimated under some assumptions (Guess et al., 2016; Zanetti et al., 2017).

In this study, for the first time, a computational multibody approach was used to compare TPLO and CBLO effectiveness in treating ACL deficient knee. First, a multibody model of a physiological knee joint was created. Secondly, starting from this model, an ACL insufficiency was reproduced. These two first models were validated on reported in vivo experimental data (Korvick et al., 1994; Lopez et al., 2003, 2004). Hence, the TPLO and CBLO surgical procedures were virtually performed. Finally, all four models (physiological, ACL-deficient, TPLO-treated and CBLO-treated) were compared to assess the effectiveness of different treatments, with reference to two loading conditions, specifically, the drawer test and the weight-bearing squat movement. Results pertaining to AP tibial translation and articular forces (i.e. compressive force, quadriceps force, patellar ligament force) were obtained and discussed. It was hypothesized that both considered surgical procedures will lead to an increase of the articular forces with respect to the physiological condition.

3.1.2 Model

With reference to the computational model implementation, it should be underlined that, (1) contact forces, (2) main muscle forces and (3) ligaments forces were considered in order to obtain reliable intra-articular forces.

Four numerical knee models were created: physiological, pathological (ACL-deficient), TPLO-treated and CBLO-treated.

The physiological model was composed by the following bones: femur, tibia, fibula, and patella (Figure 11).

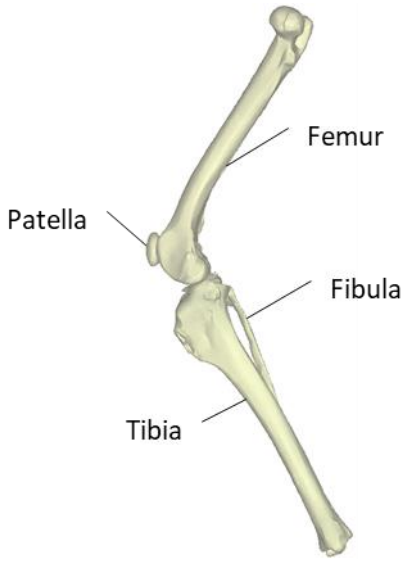

Figure 11. Bones considered in the knee model.

Bone geometries were obtained from a commercially available CAD model of a medium-sized canine knee (Sawbones® Europe AB, Malmoe, Sweden). The tibia together with the fibula were modelled as a single body (i.e. tibiofibular joints are considered as fixed joints). The patella was represented as an ellipsoid with its major length based on values found in the literature (Łojszczyk-Szczepaniak et al., 2017) and its other two perpendicular dimensions were chosen to make it congruent to the femoral groove. Given the patellar length, its vertical position with respect to other bones, on the sagittal plane, was chosen based on the mean ratio of the patellar ligament length to the patellar length itself, which is equal to 1.45 (Johnson et al., 2006).

The tibial plateau was represented by means of a flat plane with width and length equal to 36 mm and 23 mm, respectively. An average bone density of 1800 kg/m^3 was assumed and assigned to each bone (Brown et al., 2013). Physiological and ACL-deficient model geometries are identical. Both TPLO-treated and CBLO-treated models were created by modification of the ACL-deficient model according to the respective surgical procedures. TPLO and CBLO stainless fixation plates were treated as additional rigid bodies (material density of 7750 kg/m^3) attached to the tibial shaft by a fixed joint. Moreover, proximal and distal tibial fragments, resulting from the surgical treatment, were modelled as a single body.

Deformable contacts were defined by means of the Hertz's law-based formulation between the femoral condyles and the tibial plateau, and between the patella and the femoral groove. The synovial fluid, together with the cartilage, produces a significant joint lubrication. Therefore, the friction forces between the articular surfaces were neglected. Contact parameters were tuned starting from values reported in the literature (Bertocci et al., 2016). Table 1 reports the final values used for contacts' implementation.

Table 1. Value of contact stiffness (K), the nonlinear power exponent (e), maximum damping constant (C_{max}), maximum penetration constant (δ_{max}).

Parameter	*Value*	
Stiffness (K)	1000	N/mm$^{1.5}$
Max damping (C_{max})	1	Ns/mm
Max penetration (δ_{max})	0.01	mm
Power exponent (e)	1.5	

The quadriceps and the gastrocnemius muscle were included into the models. The quadriceps muscle was connected at the upper side of the patella. The gastrocnemius was included in accordance with a common experimental setup reported in the literature (Kanno et al., 2019; S. E. Kim et al., 2010; Ramirez et al., 2015; Warzee et al., 2001). A single insertion point for the gastrocnemius was chosen just above the intercondylar fossa at the midpoint between the rear surfaces of the medial and lateral epicondyle of the femur. During the weight-bearing squat simulation, quadriceps and gastrocnemius muscles act as traction forces which avoid the collapse of the joint by counterbalancing the upper body weight. A PID controller generates the required muscle force comparing the measured vertical position and velocity of the femoral head with two respective time-dependent setpoints. Such setpoints are varied over time so that the desired squat movement is performed starting from a stable physiological stance angle of 135°. The PID controller was tuned by means of the Ziegler-Nichols tuning method obtaining the following K gains: $K_p = 300$, $K_i = 6000$, $K_d = 10$. The same K values were used for all simulated configurations.

The gastrocnemius force is derived from the PID output according to a scaling factor equal to the ratio between the muscles physiologic cross-sectional areas (PCSA). In detail, this scaling factor results equal to 0.61 for a quadriceps PCSA of 70.5 cm^2 and a gastrocnemius PCSA of 43.0 cm^2 (Williams et al. 2008).

Furthermore, the following ligaments were included in the physiological model: anterior cruciate ligament (ACL), posterior

cruciate ligament (PCL), lateral collateral ligament (LCL), medial collateral ligament (MCL), patellar ligament (PL), medial femoropatellar ligament (MFPL) and lateral femoropatellar ligament (LFPL).

The ACL, PCL, LCL and MCL were split into two bundles, in detail: MCL anterior (aMCL) and posterior (pMCL) bundle; ACL anteromedial (aACL) and posterolateral (pACL) bundle; PCL anterolateral (aPCL) and posteromedial (pPCL) bundle. This allows considering the ligament structure in bundles with their different constraining contribution. In Figure 12 are represented the positions of the attachment points and the bundles orientations of each ligament. In ACL-deficient, TPLO-treated and CBLO-treated models, the ACL ligament was excluded. Origin and insertion points were determined from anatomical references (Carpenter and Cooper, 2000).

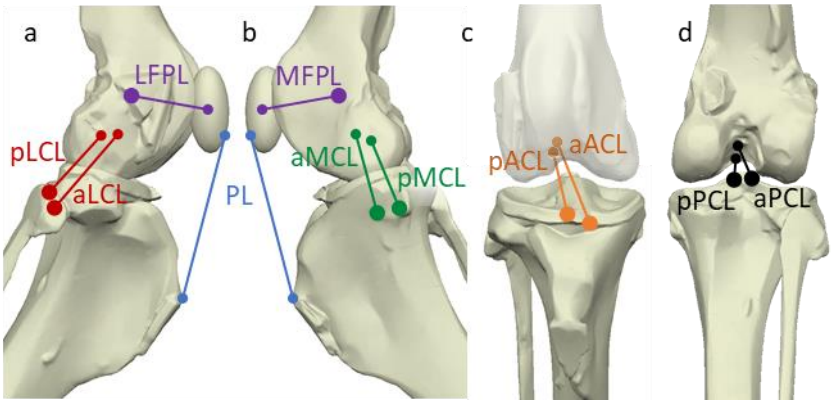

Figure 12. Different views of the knee model with the schematic representation of the included ligaments. (**a**) Lateral view; (**b**) medial view; (**c**) frontal view without the patella; (**d**) Posterior view; PL in blue; MFPL and LFPL in violet; LCL anterior (aLCL) and posterior (pLCL) bundles in red; MCL anterior (aMCL) and posterior (pMCL) bundles in green; ACL anteromedial (aACL) and posterolateral (pACL) bundles in orange; PCL anterolateral (aPCL) and posteromedial (pPCL) bundles in black.

All *k* stiffness parameters are listed in Table 2 (Brown et al. 2013). The patellar ligament was assumed to act as an inextensible element and, therefore, it was provided with a stiffness value significantly higher than all other ligaments (Haut et al. 1992).

Table 2. Stiffness parameters (expressed as force per unit strain) for each ligament bundle.

Ligament bundle	*k (N)*
aACL	3010
pACL	3010
aPCL	4460
pPCL	4460
aLCL	2280
pLCL	2280
aMCL	3445
pMCL	3445
PL	11200
MFPL	2800
LFPL	2800

The zero-load length l_0 was determined for each ligament bundle throughout a series of preliminary simulations. First, all bone segments were positioned at 135° extension so that articular surfaces matched, according to anatomical references. The femur was kept fixed in space as well as the patella in the femoral groove, while the tibia-fibula complex was constrained to maintain the 135° extension on the sagittal plane. Muscles, cruciate and collateral ligaments were deactivated at this stage. The static equilibrium conditions of the model were calculated by applying a 10 N upward force, at the tibia center of mass (COM).

Zero-load lengths were determined in this configuration as the straight-line distances between origin and insertion points of each ligament. Successively, cruciate and collateral ligaments were activated and the previously obtained zero-load lengths (initial lengths) were iteratively refined performing the drawer test simulation, on both physiological and ACL-deficient models, in order to fit AP tibial translations reported in experimental outcomes (Lopez et al. 2003, 2004; Korvick et al. 1994). It is important to note that the so found zero-load lengths (final lengths) were kept constant for all considered models.

The constraining forces due to the menisci were simulated. The stiffness of these springs was set equal to 10% the values reported for human menisci, that are 5 N/mm and 7 N/mm for the AP and mediolateral direction, respectively (Li et al., 1999).

3.1.3 Surgical procedures

First, the pre-operative TPA was defined by measuring the angle formed between the slope of the medial tibial condyle and the perpendicular to the diaphyseal tibial axis that is, in turn, defined as the line passing through the middle point between the anterior and posterior cortex at the distal 50% and 75% of the tibial shaft length (Osmond et al., 2006). The analyzed tibial geometry presented a pre-operative TPA equal to about 27° (Figure 13a). The TPLO was performed starting from the physiological model of the canine knee. The TPLO involves the rotation of the proximal tibia to achieve a suggested post-operative TPA of 5° (Figure 13b). A circular cut is created in the proximal tibia and then the bone fragment is rotated until the

tibial plateau reaches the desired angle. In this study, a 24 mm radius was chosen to produce the cut that was centered over the intercondylar tubercles to maintain enough bone in the proximal segment for an adequate fixation (Kim et al., 2008). The CBLO was performed starting from the physiological model of the canine knee, as well. The position of the CORA is located at the intersection between the proximal tibial axis and the diaphyseal tibial axis where the former is obtained as a line passing through the intercondylar tubercles having a posterior angle of 80° from the tibial plateau plane Figure 13a. The osteotomy was centered slightly cranially with respect to the CORA (Figure 13c). The exact distance of the osteotomy center from the CORA point was calculated according to the surgical procedure (Raske et al., 2013) and resulted to be equal to 7 mm. The CORA angle is defined as the angle between the proximal tibial axis and the diaphyseal tibial axis. The osteotomy radius was set equal to 18 mm, according to surgical directives that recommend a cut diameter slightly larger than the diameter of the tibial transversal section at the CORA. This surgical procedure aims to reach a post-operative TPA ranging between 9° and 12°, through the alignment of the proximal and diaphyseal tibial axes, that is, setting the CORA angle equal to 0°. In this study, the post-operative TPA has resulted to be equal to 10° (Figure 14d). Finally, the two portions of the osteotomy are kept in position by TPLO and CBLO plates, respectively (Figure 14c-d).

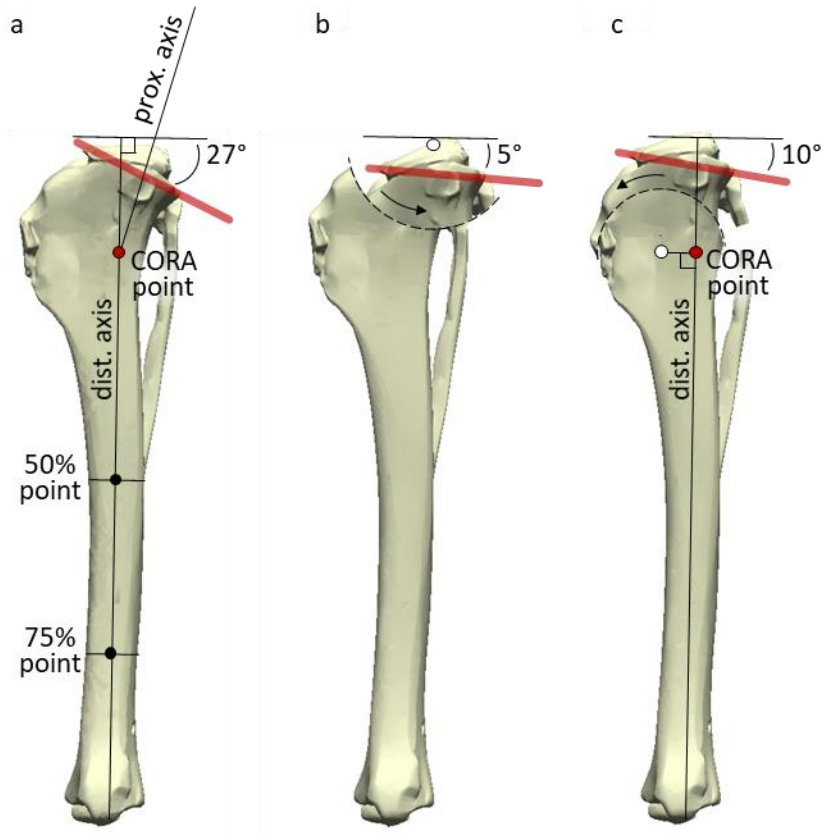

Figure 13. (**a**) Physiological tibia-fibula complex showing distal and proximal tibial axes and the CORA point (red dot); (**b**) TPLO procedure; (**c**) CBLO procedure. The tibial plateau (red lines) with its angle, the osteotomy centre (white dot) and cut (dashed line) are also showed.

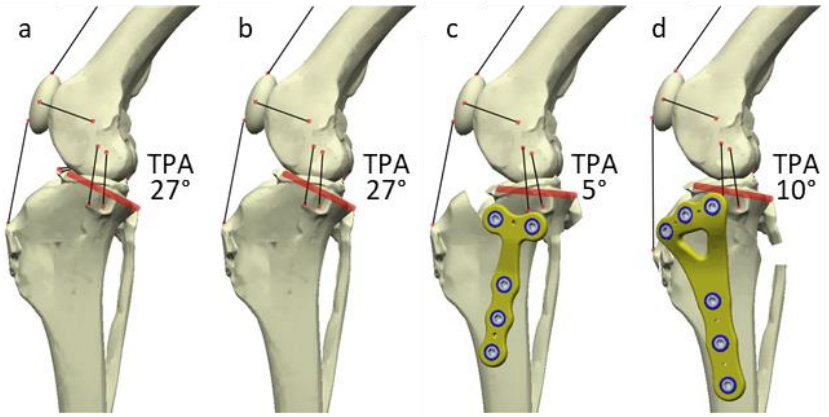

Figure 14. (**a**) Physiological model; (**b**) Pathological model; (**c**) TPLO-treated model; (**d**) CBLO-treated model. Transparent red lines show the tibial plateau. The CBLO and TPLO plates used (Fixin, Intrauma S.p.A., Rivoli, Italy) are shown in yellow. The final tibial plateau angle (TPA) is also reported.

3.1.4 Drawer test simulation

Drawer test simulation was performed with a dual aim: firstly, it was used to validate the physiological and pathological models by comparison with data from previously reported *in vivo* experiments (Korvick et al., 1994; Lopez et al., 2003, 2004); secondly, it was used to assess the effect of the two alternative surgical treatments. No muscle activation is supposed to take place during the drawer test simulation; therefore, muscles were deactivated for this simulation as well as the patella and its related ligaments (PL, MPFL and LPFL), since their exclusive function is transferring the quadriceps traction force to the tibial bone segment. The ACL was active only in the physiological case. The hind limb was fixed by fully constraining the femur (Figure 15).

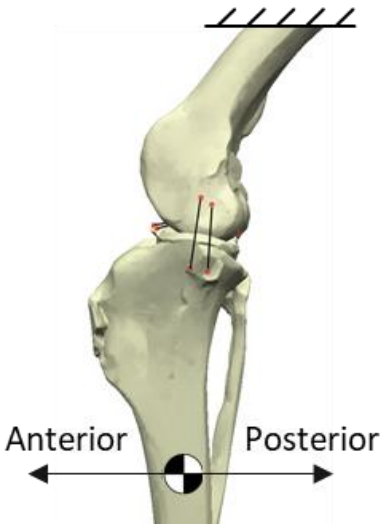

Figure 15. Model configuration for the drawer test with the knee at 135° extension and the femur fixed in place.

At the beginning of the simulation, the tibia-fibula complex was forced to maintain a 135° extension angle. Once the equilibrium was reached, one more constraint was added, forcing the tibia-fibula complex to move on the sagittal plane. The drawer test was performed applying a forward/backward force at the tibia COM. In detail, the force trend over time was defined by a smooth step function (i.e. polynomial Heaviside step function approximation), which increases up to 40 N or decreases up to -40 N (at a rate of about 2.1 N/s) to obtain the anterior or posterior drawer motion, respectively. During the drawer test, the AP tibial translation was measured as the displacement of the tibial COM along the direction perpendicular to the tibial longitudinal axes. This measure is referred to the equilibrium position, that is, the position that the knee assumes at the beginning of the simulation, when the drawer force has not been applied yet. Then, the measured AP tibial translations were compared with data from previously reported *in vivo* experiments (Lopez et al. 2003, 2004; Korvick et al. 1994).

3.1.5 Squat simulation

To reproduce the *in vivo* four-legged stance condition during a weight-bearing squat movement, the gravitational field was included in the model and applied along the vertical direction. The upper end of the hind limb was constrained to a spherical joint, whose center was coincident with the femoral head center. This joint was left free to translate along the vertical direction (Figure 16a) as a result, the femoral head moved along a vertical axis during the squat movement.

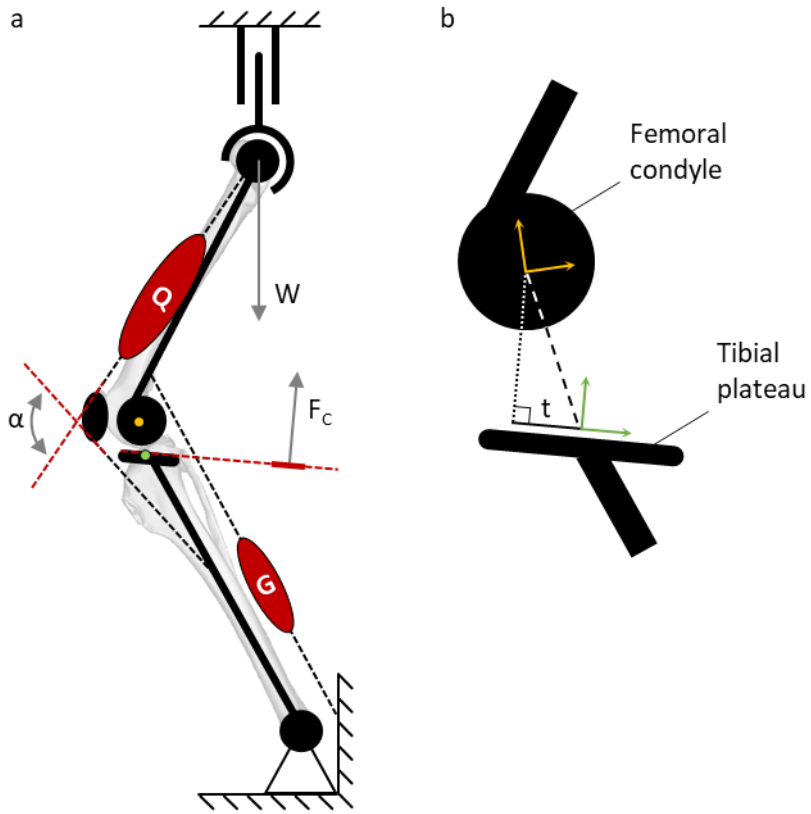

Figure 16. (**a**) 2D schematic diagram of the knee which shows constraints, muscles (Q: quadriceps; G: gastrocnemius), body weight (W) and the angle between the quadriceps and patellar ligament action lines (α). The compressive articular force (F_C) is shown with its direction, and the markers used to measure the cranial tibial translation are also shown (green and yellow dots). (**b**) Detail of the markers used to measure the AP tibial translation (t).

The limb was constrained to the ground through a revolute joint, at its lower end. This joint was located at the center of the medial malleolus and its axis of rotation was set perpendicular to the sagittal plane. The body-mass acting on the limb was located at the upper joint center and it was set equal to 10 kg, which corresponds to 30% of the average body weight of a middle size dog (S. E. Kim et al., 2009). The squat movement was obtained through the PID controller, which generates the muscle force

required to perform the knee flexion. Hence, the model was free to determine its own kinematics during the simulation. The AP tibial translation during squat simulation was measured as the projection on the tibial plateau of the line connecting two markers, one on the femur and the other one on the tibia (Figure 16b). In detail, the femur marker is located at the center of the sphere inscribing the medial femoral condyle, whereas, the tibial marker is located on the tibial plateau at the center of the medial condyle. The AP tibial translation results to be positive or negative when the tibial marker lies anteriorly or posteriorly with respect to the femoral marker, respectively. In particular, squat simulation focused on the assessment of the AP tibial translation, the compressive articular force, the generated quadriceps force as well as the patellar ligament force. Moreover, the angle α defined between the projections on the sagittal plane of the quadriceps line of action and of the patellar ligament line of action was measured at the beginning (135°) and at the end (90°) of the flexion movement.

3.1.6 Results

The ligaments refinement led to an average variation of about 6.8% of the initial zero-load lengths (Table 3).

Findings related to the drawer test simulation revealed that ACL-deficiency causes an increase of the anterior tibial translation, that is, from 1.1 mm to 6.3 mm (Figure 17).

Total AP translation ranges equal to 2.3 mm and to 7.5 mm were found for the physiological model and the pathological one, respectively.

Table 3. Initial and final zero-load lengths (l_0) for each ligament bundle.

Ligament bundle	*Initial l_0 (mm)*	*Final l_0 (mm)*	*Length change (%)*
aACL	24.7	26.9	+8.9
pACL	20.7	23.4	+13.0
aPCL	8.3	9.1	+9.6
pPCL	9.4	10.3	+9.6
aLCL	23.6	20.8	-11.9
pLCL	19.7	16.5	-16.2
aMCL	20.7	20.1	-2.9
pMCL	19.2	18.6	-3.1
PL	38.1	38.1	0
MFPL	22.3	22.3	0
LFPL	24.1	24.1	0

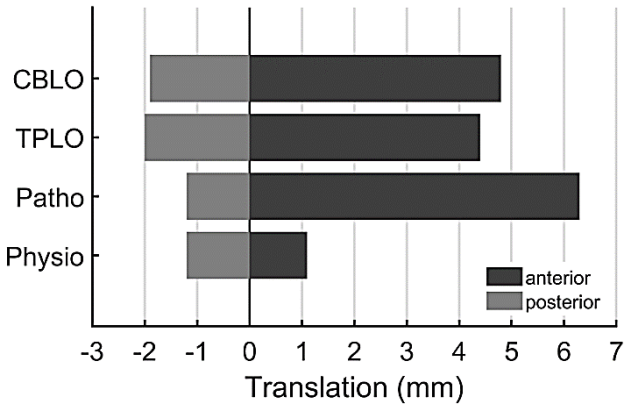

Figure 17. Anterior and posterior translations of the tibia relative to the femur, resulting from the drawer test simulation, performed on all models: CBLO-treated (CBLO), TPLO-treated (TPLO), Pathological (Patho), and Physiological (Physio). The vertical zero line is the equilibrium position reached by each model before the application of the AP drawer force.

After surgical treatments, the anterior tibial translation, caused by ACL-deficiency, undergoes a reduction of about 1.5 mm at the expense of the posterior translation, which increases.

Overall, no appreciable differences between CBLO-treated model and TPLO-treated model are evident from the drawer test. Initial and final knee configurations obtained from squat simulations are depicted in Figure 18.

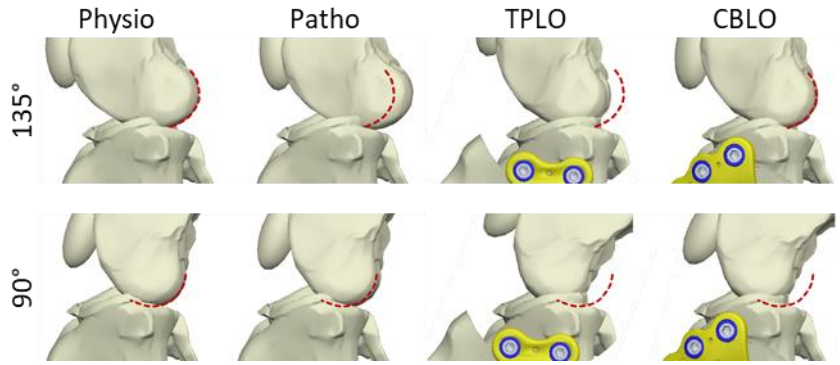

Figure 18. Initial (top) and final (bottom) relative positions between the femur and the tibia, for the four considered models, during the squat simulations. The different configurations are aligned referring to the tibial plateau. Red dashed lines report the femoral condyle position in the physiological case.

In details, ACL-deficiency resulted in anterior tibial translation of 5.6 mm at 135° (Figure 19). Conversely, at the same extension angle, a posterior tibial translation equal to 1.2 mm or even equal to 4.8 mm take place in CBLO- and TPLO-treated model, respectively. In addition, the initial anterior tibial translation in the pathological model is almost completely recovered over the entire flexion arch, reaching a value equal to 1.1 mm at the flexion end. Vice versa, the initial posterior tibial translation in the CBLO-treated model increases over the full flexion range, reaching a value equal to 4.8 mm at 90°. As regards the TPLO-treated model, the initial posterior tibial translation is essentially maintained constant over the whole

flexion range, increasing from 4.8 mm to a maximum value equal to 5.6 mm.

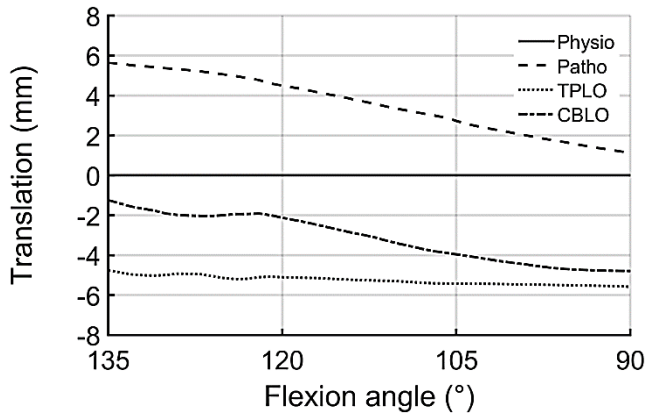

Figure 19. AP tibial translations during the squat simulation. The horizontal zero line represents the physiological condition (Physio). Positive and negative translation values reflect anterior and posterior tibial displacements referred to the physiological one.

The traction force generated by the quadriceps muscle changes considerably among the four configurations (Figure 20). The quadriceps force computed at 135° is about 165 N for all models except for the CBLO, which presents a higher force equal to 196 N. In detail, the muscle forces, in the TPLO-treated model and the physiological one, are coincident for flexion angles ranging between 135° to about 105°. However, for smaller flexion angle, the muscle force increases faster for the TPLO-treated model compared to the physiological one. Overall, the highest quadriceps force, equal to 973 N, was found for the CBLO-treated model. Similarly to the quadriceps force trends, the highest patellar reaction force was found in the CBLO-treated model (Figure 21).

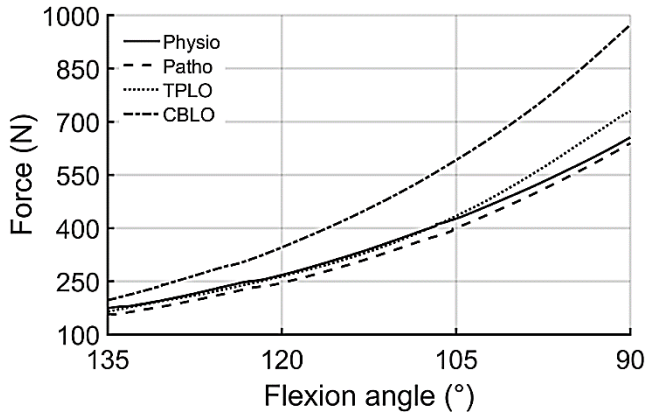

Figure 20. Quadriceps force generated by the PID controller during the squat simulation.

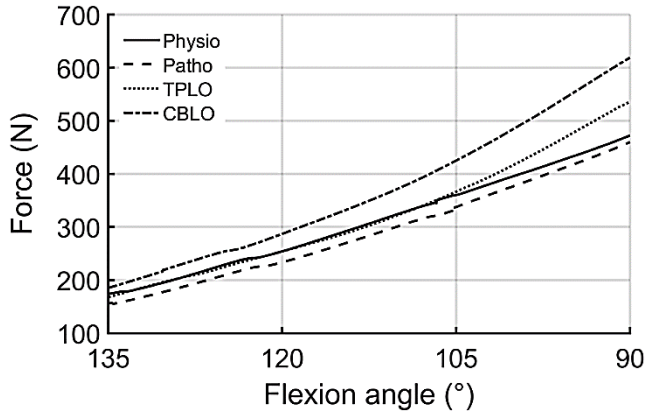

Figure 21. Patellar ligament reaction force measured during the squat simulation.

In all cases, the angle α decreases along with the flexion angle (Table 4). However, with respect to the physiological model, the pathological condition leads to an increase of the angle equal to 4.7% and 1.4% at 135° and 90° flexion, respectively. On the other hand, a reversed trend results from both TPLO and CBLO models, where a narrower angle occurs and decreases over the flexion range, from -4.1% up to -5.8% for

the TPLO and from -8.8% up to even -12.3% for the CBLO. With regard to the compressive articular force, the maximum value took place at 90° flexion angle and was equal to 1530 N and 1359 N for the CBLO and the TPLO, respectively, against a value equal to 995 N measured in the physiological model (Figure 22).

Table 4. Variation of the angle α, defined between the quadriceps line of action and the patellar ligament line of action, measured at the beginning (135°) and at the end (90°) of the flexion movement among the four models. Percentage of angle variation with respect to the physiological model are reported in brackets.

Model	*Flexion angle*			
	135°		*90°*	
Physiological	170°		138°	
Pathological	178°	(+4.7 %)	140°	(+1.4 %)
TPLO	163°	(-4.1 %)	130°	(-5.8 %)
CBLO	155°	(-8.8 %)	121°	(-12.3 %)

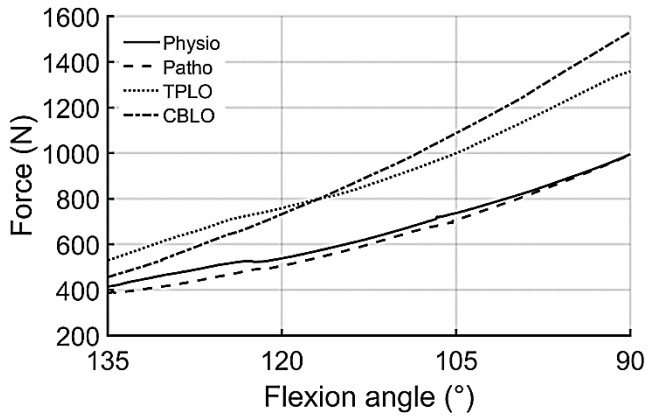

Figure 22. Compressive force representing the intra-articular contact force directed perpendicular to the tibial plateau measured during the squat simulation.

In addition, the CBLO-treated model is affected by a higher increase rate of the compressive force compared to the TPLO-treated one. As a result, the CBLO produces a lower force compared to the TPLO for flexion angles ranging from 135° to 117°.

3.1.7 Discussion

In this study, a computational multibody analysis was performed with the aim to compare TPLO and CBLO effectiveness in treating ACL deficiency under the hypothesis that both considered surgical procedures induce an increase of the articular forces with respect to the physiological condition.

The drawer test simulation confirmed that the absence of the ACL constraining force causes an increase of the anterior tibial translation. Although several studies have reported the effect of ACL rupture on tibial translation, a direct comparison of these findings was difficult due to variations in tests across studies. Nevertheless, the translational values obtained from the drawer test in this study are consistent with *in vivo* experimental data reported by Lopez et al. (2003, 2004) and Korvick et al. (1994) for pathological and ACL-deficiency conditions. In addition, our results show that both treatments produce only a slight reduction of the total AP translation range, compared to the pathological model. This was expected since both treatments aim to achieve a dynamic stabilization of the joint in a weight-bearing condition, that is, when the body weight and the muscle actions give an additional contribution to the joint stability. In the drawer test, the only stabilizing action is played by stretched ligaments; hence,

the TPA modification has a minimal impact on the total AP translation range due to tibiofemoral articular surfaces reciprocal sliding, according to the tibial slope.

As far as the squat flexion is concerned, both surgical treatments generate an inversion in the tibial translation, namely, the tibia move posteriorly with respect to the physiological condition. This same inversion was reported in TPLO-treated knees in the experimental study by Warzee et al. (2001).

Furthermore, important considerations can be drawn from an analysis of the traction force generated by the quadriceps muscle. In general, the minimum computed forces for quadriceps are lower than those reported by other experimental studies (Drew et al., 2018; Kanno et al., 2019), where, however, the application method of the emulated muscle forces is not well defined. The highest quadriceps force was found in the CBLO-treated model. This is likely to be due to the anterior translation of the femoral condyles that results in a reduction of the quadriceps moment arm (Grelsamer and Klein, 1998; Kanno et al., 2019; Schindler and Scott, 2011). Therefore, a higher muscle force is needed to obtain a given joint extension moment.

In addition, the angle (α) between the direction of the quadriceps force and the direction of the patellar ligament also plays an influence (Aglietti and Menchetti, 1995). Specifically, a lower value of this angle entails higher quadriceps forces. The lowest angle was found for the CBLO-treated model, giving a contribution to the quadriceps force increase.

The pattern of the patellar ligament force is similar to that of the quadriceps force, since these quantities are closely related, so

the higher patellar forces are produced by the CBLO procedure. On that note, it should be reminded that higher patellar ligament forces mean higher ligament stresses which, in turn, may lead to ligament thickening or desmitis (Beer et al., 2018; Mattern et al., 2006; Milovancev and Schaefer, 2009).

Overall, the basic concept behind TPLO surgery is converting tangential forces acting on the tibial plateau into a compressive reaction force, normal to the plateau itself (Slocum and Slocum, 1993). However, an excessive compressive force could lead to degenerative complications, such as osteoarthritis and meniscal injuries (Beer et al., 2018). From articular compressive forces computed during squat simulations, it is evident how the ACL-deficient knee undergoes a lower compressive articular force, compared to the physiological knee, and this is in accordance with Kim et al. (2009). In contrast, both surgical treatments cause an increase of this compressive force. As known, surgery for ACL-deficiency is performed on pathologic knees characterized by degenerated cartilage. Therefore, the higher articular compressive force in limb extension, following TPLO, should be reason for concern regarding this technique.

As a matter of fact, this study is affected by some limitations which should be highlighted. First, it should be taken into account that, due to the lack of specific reference data in literature, the physiological and pathological models were validated solely on AP tibial translations resulting from previous *in vivo* experiments involving the drawer test.

Another limit is the estimation of the gastrocnemius contribution as a fraction of the quadriceps action. Nevertheless,

it is not clear how the applied gastrocnemius force was determined throughout the experimental reference studies.

Moreover, the modelling of the patella as an ellipsoid should be avoided since this likely leads to a reduced patellofemoral joint stability. However, here the patella was considered merely as element used to transfer the quadriceps traction force to the tibial bone segment, therefore, its main dimensions were considered while secondary shape characteristics were overlooked.

Also, both the plates and screws were assumed as rigid and attached to the bone by a fixed joint. Such assumption might potentially cause an increase in the model stiffness and, consequently, in the measured tibiofemoral contact forces, even if minimally.

Finally, the present study was addressed to a short-time post-operative scenario, hence, neglecting phenomena that might occur over time due to soft tissue behaviours (e.g. stress-relaxation and recovery phenomena).

Multibody Model for Ligament Balancing in Total Knee Arthroplasty

Total knee arthroplasty (TKA) is the most common surgical procedure for treatment of chronic degenerative pathologies of the knee involving the replacement of the damaged articular surfaces of the joint with artificial components, generally, including femur component, tibial tray, and insert. A correct implant positioning, together with an optimal ligament balancing, are mandatory to achieve the best surgical outcomes. Especially, a proper tibial component slope helps to avoid increased ligament tensions and instabilities. Although, new tools for TKA were developed to provide quantitative analysis of the tibiofemoral compressive force and implant components positioning, the ligaments tensioning remains only qualitatively assessed through subjective clinical manoeuvres.

The aim of this study was the development of a multibody model of a prosthetic human knee able to give valuable information for balancing of the collateral ligaments. In particular, the traction forces generated by each ligament bundle as well as the contact forces acting on the medial and lateral knee compartments during a passive flexion were computed with different tibial tray slopes and insert thicknesses.

Initially, the ligament balancing was achieved by iteratively performing the simulation of a passive knee flexion and, simultaneously, adjusting the ligament zero-load lengths. Then, such balanced condition was taken as baseline for a series of consecutive simulations where the varus/valgus and

posterior/anterior slopes of the tibial tray were modified between ±4° by steps of 2°. In addition, the insert thickness was also varied between ±2 mm by steps of 1 mm. Finally, all simulations were compared to assess how the tibial tray slopes and insert thickness affect the ligaments traction forces and articular contact forces. In order to test the feasibility of integrating the simulation into a clinical procedure, a software interface was also implemented to easily change the implant configuration and run the simulation.

The model developed in this study has proven to be able to predict quantitative information which are in agreement with other experimental studies. In the balanced condition, the contact force difference between the medial and lateral compartments was less than 52 N with ligaments traction forces below 50 N. Results from implant variations highlight the predominant role of the insert thickness in increasing all considered forces. Moreover, the varus/valgus variation let to the highest compartmental contact force on the lateral side. Finally, a higher anterior slope resulted in higher tibiofemoral contact force and vice versa.

3.2.1 Background

Musculoskeletal disorders such as osteoarthritis, arthrosis and osteoporosis are among the main causes for disability and pain in the modern society (Zheng and Nolte, 2015). When the non-surgical treatments fail, the implant of joint prothesis after bone resection is usually suggested.

Total knee arthroplasty (TKA) is the most common surgical procedure for treatment of chronic degenerative pathologies of

the knee. TKA implies the replacement of the damaged articular surfaces of the knee with metal and plastic components. In general, total knee implants consist of three parts: femur component, tibial tray, and insert. In addition, a patellar component can be included as well. The main goals of the TKA are pain alleviation and recovery of the functional stability of the knee joint. To date, although the surgical procedure is well-established, there is still a revision risk equal to 5% at 10 years (Popescu et al., 2019).

A successful surgical outcome depends on various technical factors including proper bone resection, correct alignment of the implant components, and above all an adequate soft tissue balancing. Especially, ligament balancing plays a significant role for post-operative patient satisfaction and implant longevity (Smith et al., 2016). Indeed, excessively tight ligaments can lead to articular pain, stiffness, and reduction of the range of motion. In contrast, overly loose ligaments can generate complications associated with joint instability. Revision arthroplasty due to postoperative instability has been estimated in more than 20% per year (Cho et al., 2018). In addition, misalignment and imbalance can produce a concentration of the tibiofemoral loads which could trigger wear phenomena at the contact interfaces, thus, shortening the implant lifetime.

Traditionally, to achieve an appropriate balance, surgeons can adjust implant alignment or perform soft tissues releases. However, these methods typically rely on the surgeon's experience and his subjective evaluations.

Driven by the need to minimize the complications caused by the subjectivity of ligament balancing, in the last decades, a series of mechanical devices able to provide quantitative intra-operative measurements of the ligament balancing have been developed. Some commercially available devices are eLIBRA (Zimmer Inc., Warsaw, USA) and Verasense (OrthoSensor Inc., Dania Beach, FL). These devices allow to quantify medial and lateral tibiofemoral compressive force. In particular, Verasense can also localize the contact points of the femoral condyles on the insert surface. Moreover, thanks to the introduction of computer-assisted orthopaedic surgery (CAOS) approaches, which involve the adoption of increasingly sophisticated navigation and robotic systems during the surgical process, the accuracy of three-dimensional implant alignment can be also improved.

Although all these devices and systems provide more quantitative analysis of the factors that contribute for a better surgical outcome, forces exerted by the ligaments remain only qualitatively assessed by means of manual trial movements. In fact, the intra-operative measurement of the ligament forces throughout the flexion motion is still an open challenge. In order to address the lack of information related to the compressive and tensile state of the soft tissues, the integration of biomechanical simulations into the surgical procedure appears as a very interesting approach to investigate. Recently, some attempts have been made to include biomechanical simulations into the surgical decision-making process for orthopedic interventions. For instance, a biomechanical guidance system was proposed by Armand and co-workers (Armand et al., 2018) to intraoperatively

simulate different tasks scenarios (e.g., walking, sitting), thus, predicting the contact pressure distribution in the hip joint with the aim to optimize the joint alignment for performing a periacetabular osteotomy. It should be noted that the implementation of patient-specific models is complex, since they require the knowledge of detailed anatomical information as well as the mechanical properties of the involved biological tissues. However, the development of a properly simplified model, coupled with the aforementioned sensing devices and CAOS systems, could lead to a better understanding of the joint biomechanics as well as provide more effective information to support surgeons during the preplanning and intraoperative phases.

Aim of this study was the implementation of a multibody model of a prosthetic knee able to predict the traction forces exerted by the collateral ligaments throughout a passive knee flexion. Furthermore, medial and lateral tibiofemoral contact forces were also computed at the interface between the femoral component and insert. In addition, a custom-made software interface was implemented to interactively modify the insert thickness and tibial tray slopes on both the coronal and sagittal planes, thereby, investigating how such variations impact on the tibiofemoral contact forces and ligaments forces.

3.2.2 Model

The multibody model of a prosthetic left knee (Figure 23) was created by assembling commercially available geometries of the femur and tibia bones (Sawbones® Europe AB, Malmoe,

Sweden) together with a total knee prosthesis (Gruppo BioImpianti s.r.l., Milan, Italy). The distal femur and proximal tibia geometries were properly cut in order to host the femoral and tibial implant components, respectively. In addition to the femoral and tibial metal components, a polyethylene (UHMWPE) insert completes the prosthesis assembly.

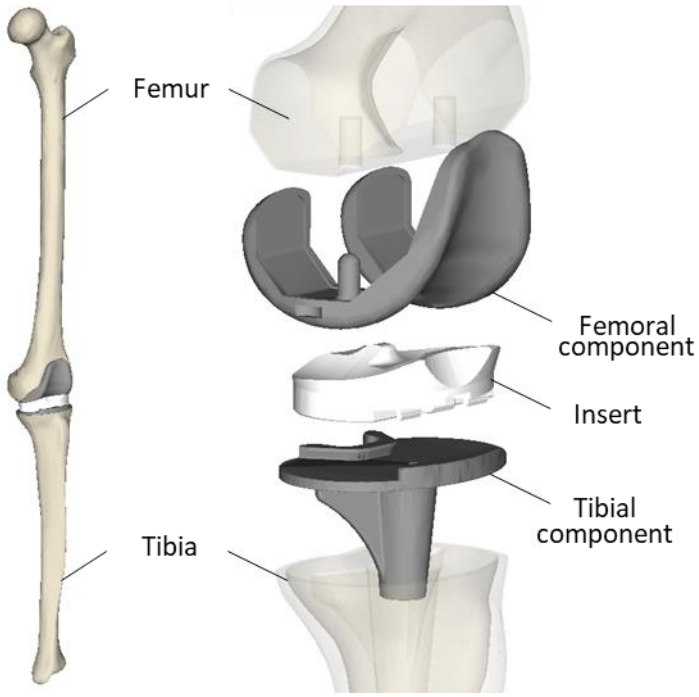

Figure 23. On the left, the prosthetic knee model. On the right the exploded view showing the implant components.

The insert consists of polyethylene (UHMWPE) and presents a posterior stabilized design characterized by a symmetrical mediolateral shape. In order to distinguish between medial and lateral tibiofemoral contact force, the insert geometry was split along its sagittal plane obtaining two symmetrical rigid bodies.

Then, each insert part was rigidly fixed on the tibial component, thereby, neither relative rotation nor translation between tibial component and insert are allowed. An average density of 1000 kg/m^3 and 2740 kg/m^3 was assumed and assigned to the femoral and tibial bone, respectively, whereas a density of 4850 kg/m^3 and 960 kg/m^3 was assigned to each of the implant metal component and polyethylene insert, respectively.

Deformable contacts were defined by means of the Hertz's law-based formulation between the femoral component and each of the two insert parts. The friction force between the articular surfaces was considered, specifically, values equal to 0.03 and 0.01 were used as static and dynamic friction coefficient, respectively (Stylianou et al., 2013). Contact parameters were tuned based on the method describe before (see paragraph 2.3.3). Table 5 reports the final values used for contacts implementation. Moreover, the medial (MCL) and lateral (LCL) collateral ligaments were included in the model. Each ligament was further split into three bundles, in detail: MCL anterior (aMCL), intermediate (iMCL) and posterior (pMCL) bundle; LCL anterior (aLCL), superior (sLCL) and posterior (pLCL) bundle.

Table 5. Value of contact stiffness (K), the nonlinear power exponent (e), maximum damping constant (C_{max}), maximum penetration constant (δ_{max}).

Parameter	*Value*	
Stiffness (K)	72800	N/mm$^{2.5}$
Max damping (C_{max})	966	Ns/mm
Max penetration (δ_{max})	0.01	mm
Power exponent (e)	2.5	

This division allows considering the ligament structure in bundles with their different constraining contribution. In Figure 26 are represented the positions of the attachment points and the bundles orientations of each ligament. Origin and insertion points were determined from anatomical references. Table 6 reports all considered ligaments bundles with the related stiffness parameters *k* which were adopted from literature (Marra et al., 2015).

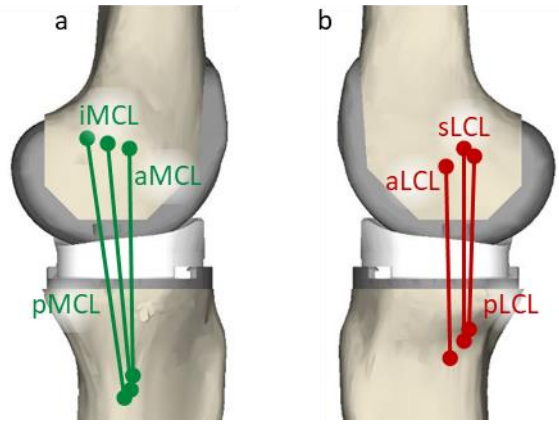

Figure 24. (**a**) Medial view of the knee model in extension showing the medial collateral ligament bundles; (**b**) Lateral view of the knee model showing the lateral collateral ligament bundles.

Table 6. Stiffness parameters (expressed as force per unit strain) for each ligament bundle.

Ligament bundle	*k (N)*
aMCL	2750
iMCL	2750
pMCL	2750
aLCL	2000
sLCL	2000
pLCL	2000

The zero-load length of each ligament bundle was tuned by iteratively performing the simulation of a passive knee flexion and simultaneously adjusting the ligament zero-load lengths following the strategy propose by Guess and co-workers (Guess and Razu, 2017) which involves two assumptions: during the passive movement of the knee throughout its range of motion (1) every ligament bundle is stretched, and (2) the force exerted by each bundle should be below 50 N. In particular, in this work, the zero-load lengths were iteratively corrected by steps of 1% with respect to the initial zero-load lengths until the two assumptions were satisfied.

Furthermore, also the attachment points of the bundles were modified to agree with the reported recruitment patterns of the bundles (Blankevoort, Huiskes et al., 1991).

To take into account the total weight of the tibial segment, including soft tissue masses, an ellipsoidal body was rigidly attached to the tibial bone. Mass and position of this additional body were derived from the total body weight (Tözeren, 2000) considering a male subject of 66.7 kg.

3.2.2.1 Passive flexion simulation

In order to assess the model behavior, a passive flexion simulation was carried on by means of a desktop workstation (CPU i7-6700 @ 3.4 GHz, RAM 32 GB). A bushing element is used as expedient to prescribe a specific motion into the model, that is, the passive knee flexion ranging from 5° extension up to 110° flexion (Figure 25).

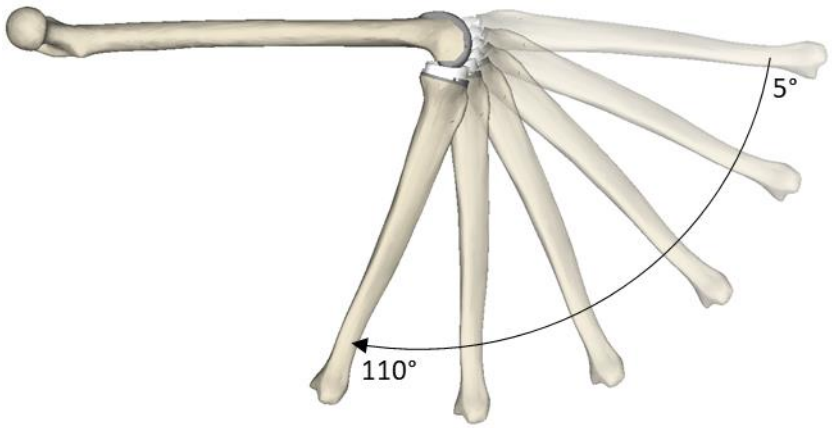

Figure 25. Passive flexion motion of the prosthetic knee model.

At the beginning of the flexion movement, the femoral and tibial segments are horizontally aligned with respect to the gravitational field. The femur is fixed in space, whereas the tibial segment kinematic is only restrained by the contacts and ligaments forces, proximally, and by a properly defined bushing element, distally. In detail, the bushing element is defined between a reference part, rigidly attached to the distal tibial segment, and a dummy part connected to the ground of the model through a revolute joint located in the middle of the femoral condyles, perpendicularly to the sagittal plane. Initially, the reference part and the dummy part are overlapped. Then, when an angular motion is prescribed at the revolute joint, the dummy part moves and, consequently, the bushing element generates a force which is proportional to the distance between the reference part and the dummy part (Figure 26). As result, the dummy part brings the tibial segment along the flexion trajectory up to the desired final angle. The simulation automatically stops when the

target flexion angle of 110° is reached. This method allows to apply the desired motion with regardless to the value of the force needed to accomplish the motion itself. In addition, undesired constraints that could affect the flexion motion of the tibia are minimized as well as the measured tibiofemoral contact force.

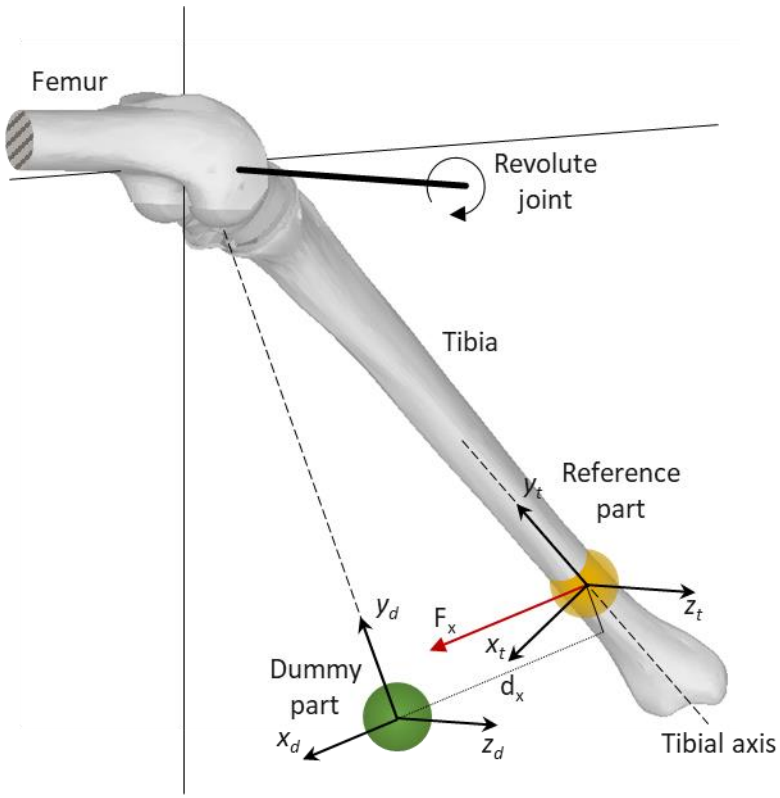

Figure 26. Schematic diagram of the motion agent used to perform the passive knee flexion. The force (F_x), generated by the bushing, is applied to the tibia along the x axis of the local reference system on the dummy part (green sphere). The force magnitude is proportional to the distance (d_x) between the reference part (orange sphere) and the dummy part, measured along the previous x axis. In the picture, for sake of clarity, the distance d_x is oversized.

3.2.3.2 Implant variation

Once the zero-load ligament lengths were optimized, the resulting knee model was taken as balanced configuration to investigate the impact of the insert thickness and tibial tray slope variation on the tibiofemoral contact forces and ligaments forces. In particular, the insert thickness was varied between ±2 mm by steps of 1 mm, whereas the varus/valgus and posterior/anterior slopes of the tibial component were modified between ±4° by steps of 2°. In the model, the insert distance from the upper surface of the tibial tray was increased and decreased (i.e. allowing bodies interpenetration) to emulate a higher and lower insert thickness variation, respectively. Similarly, the tibial component was tilted, regardless to the bone interpenetration, with respect to a point centered on the tibial tray (Figure 27).

Moreover, a custom-made software interface was implemented (Figure 28) to interactively modify the implant parameters of the model.

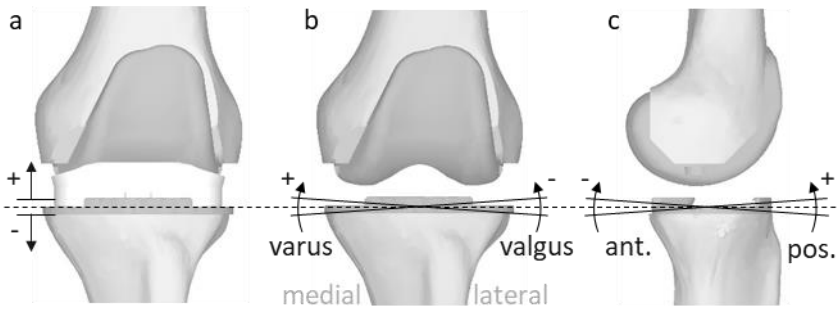

Figure 27. (**a**) Insert thickness variation, (b) tibial component slope variation on the coronal plane and (c) on the sagittal plane.

In addition, the interface allows for rapidly setting the model view on the coronal or sagittal plane, starting and stopping the simulation and visualize the simulation results as well.

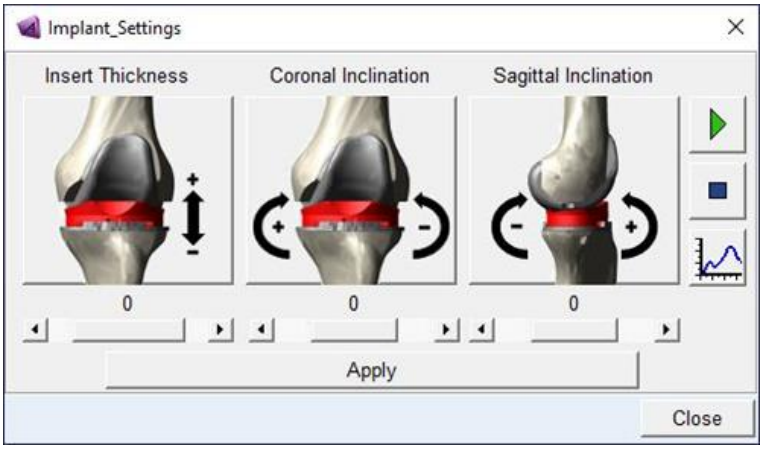

Figure 28. Custom-made software interface implemented to interactively modify the implant parameters.

3.2.4 Results

The initial ligament refinement allowed obtaining the balanced knee model which was considered as baseline to assess the impact of the different implant variations in terms of generated ligaments forces and tibiofemoral contact forces. As regards the ligament optimization process, all the obtained bundles traction forces resulted below 40 N, except for the pMCL and iMCL, which reached a maximum of about 45 N (Figure 29). In particular, it is possible to note that the same lateral and medial bundles present similar trends during the passive flexion. Indeed, the anterior bundle forces decrease from 5° to 55° and 35° for

lateral and medial ligament, respectively. The sLCL and iMCL forces are stable over the first 50° flexion, then decrease to zero at about 95°. In contrast to the posterior bundles, the aLCL and aMCL act over deeper flexion angles, reaching their maximum force at 93° and 73°, respectively, after that, it undergoes a partial decrease.

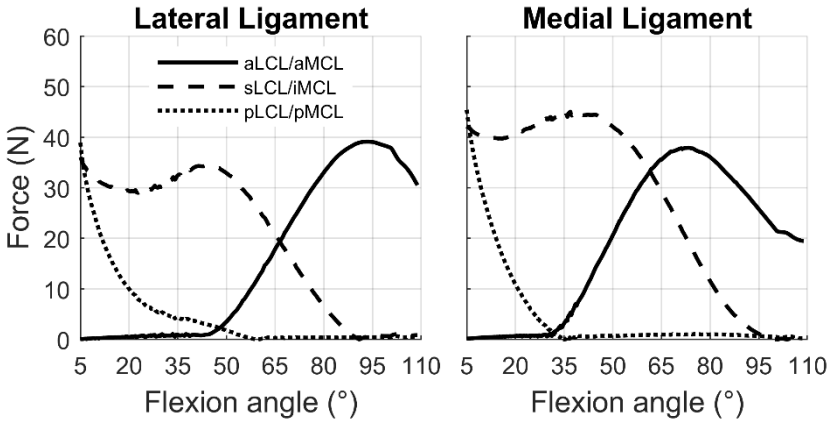

Figure 29. Ligament traction forces resulting from the balanced condition.

Looking at the tibiofemoral contact in the balanced condition, medial and lateral forces are highest at 5°, precisely equal to 89 N and 74 N, respectively (Figure 30). The medial force is higher than the lateral one from 5° up to 85°, after that, the force trend changes, indeed, the lateral force stays stable around 27 N, whereas the medial force goes down to zero at 100°. Furthermore, the highest mediolateral difference resulted equal to 52 N at about 58°.

In general, starting from the balanced model, each simulation performed by changing the considered implant parameters took less than 5 s in terms of elapsed computational time.

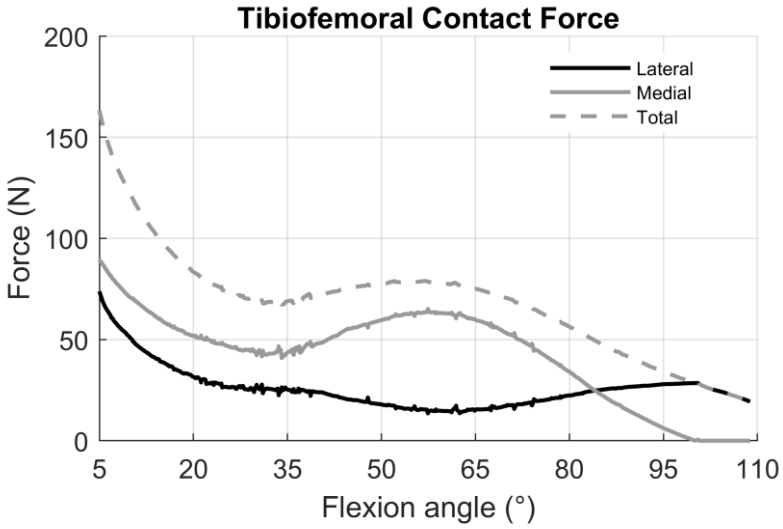

Figure 30. Lateral, medial and total tibiofemoral contact forces resulting from the balanced condition.

As far as results concerning implant variation, it can be seen that valgus and varus slope modifications mainly generate an increase in the lateral and medial ligament forces, respectively (Figure 31).

The trends of the forces exerted by the bundles for different slopes of the tibial component on the sagittal plane are similar to the reference ones (Figure 32). In this case, the highest force difference corresponds to the sLCL, showing a force value equal to only 1.5 times the related reference value.

As regards the insert thickness, medial and lateral ligaments are equally affected by an increase or decrease in the bundle force due to the insert thickening and thinning, respectively (Figure 33). In particular, only the iMCL presents slightly higher forces than the contralateral sLCL with respect to the same insert variations. However, the insert thickening causes more significant

forces changes than inserts thinning, especially, for +2 mm the pLCL force is 3.3 times higher than the related reference force at 5° flexion.

Figure 34 helps in directly visualizing the impact of each implant variations on the compartmental contact forces. The highest contact force, equal to 331 N, was generated by the 4° valgus slop in the lateral compartment at the flexion beginning. However, looking at the total tibiofemoral contact force, the 2 mm insert thickening leads to the highest value of 472 N, followed by a value of 307 N obtained for the 1 mm insert thickening. Such increases correspond to 2.9 and 1.9 times the total tibiofemoral contact force measured in the balanced model. The anterior/posterior slope variation produces the smallest contact force variation, especially on the medial compartment. In particular, a higher anterior slope leads to higher contact forces and vice versa. In this case, the maximum increase is equal to 1.5 times the reference value in the lateral compartment at the flexion beginning.

Furthermore, it can be noted that both varus slope variations imply even no contact over the whole flexion on the lateral side, whereas the valgus slops led to a reduced contact range on the medial side. In detail, the medial contact gets lost at 90° and 53° for 2° and 4° valgus slope, respectively. Insert thinning almost nullify the contact force around 70°, whereas on the medial side the contact is maintained, except for the last 10° flexion. Finally, the anterior/posterior slop variations do not cause contact losses, except for the last 10° flexion on the medial side.

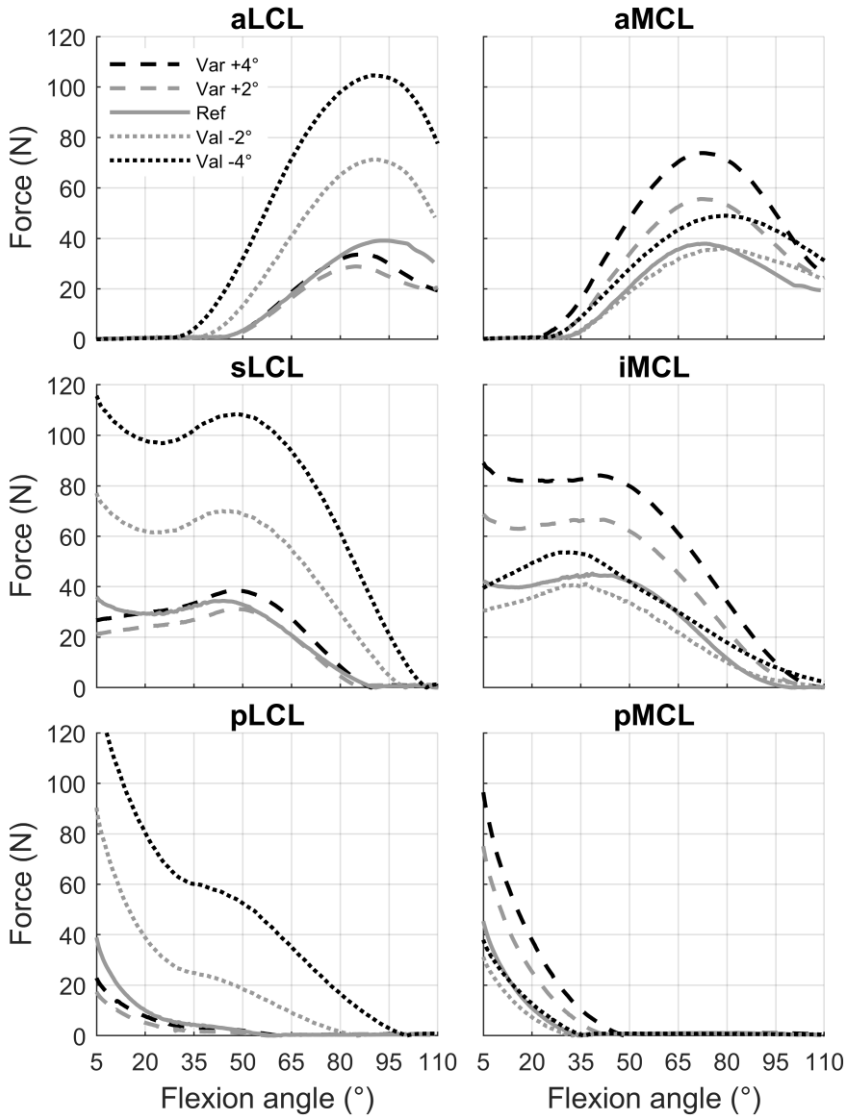

Figure 31. Impact of the tibial component varus/valgus tilt on the lateral and medial ligament forces.

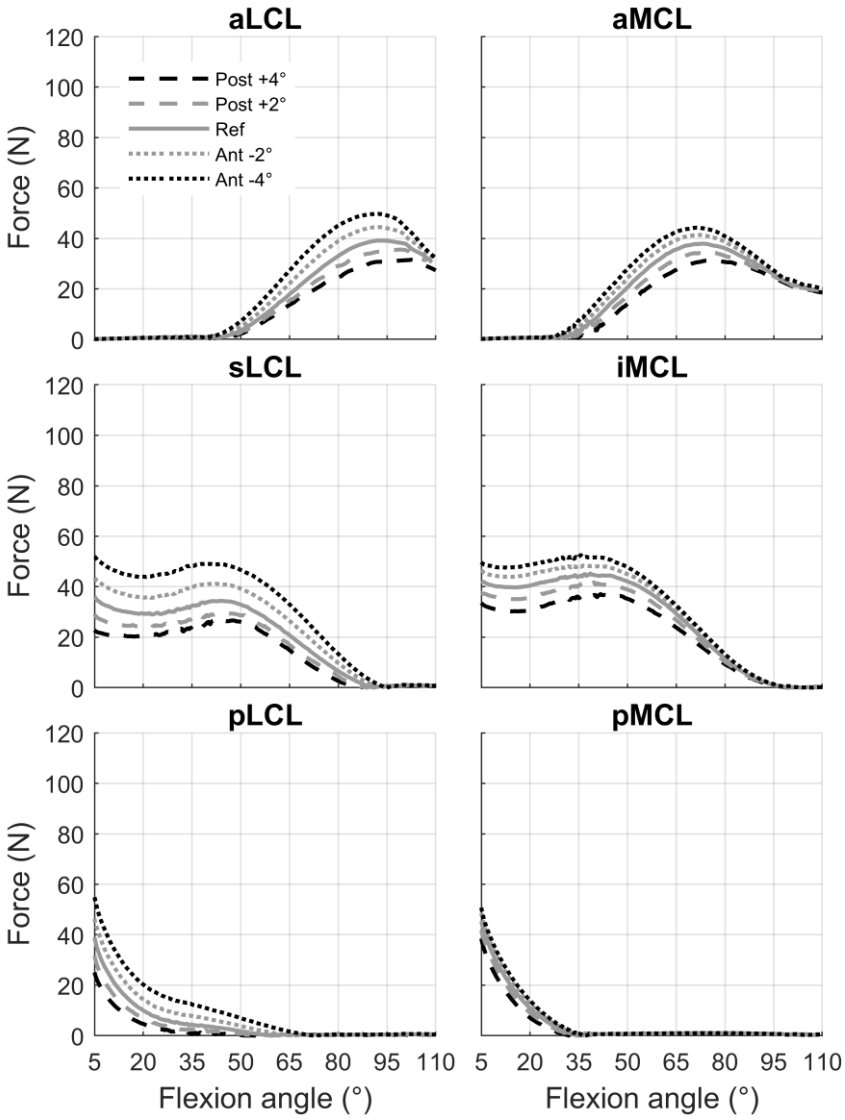

Figure 32. Impact of the tibial component anterior/posterior tilt on the lateral and medial ligament forces.

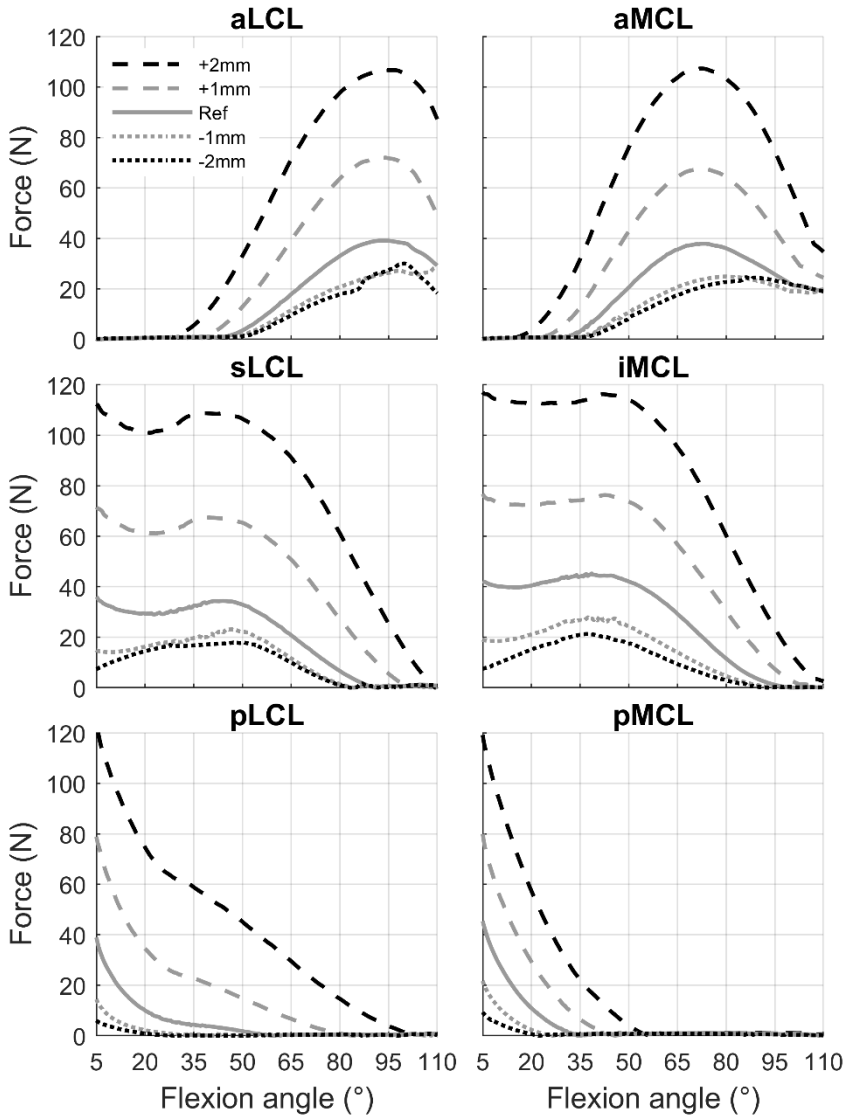

Figure 33. Impact of the insert thickness on the lateral and medial ligament forces.

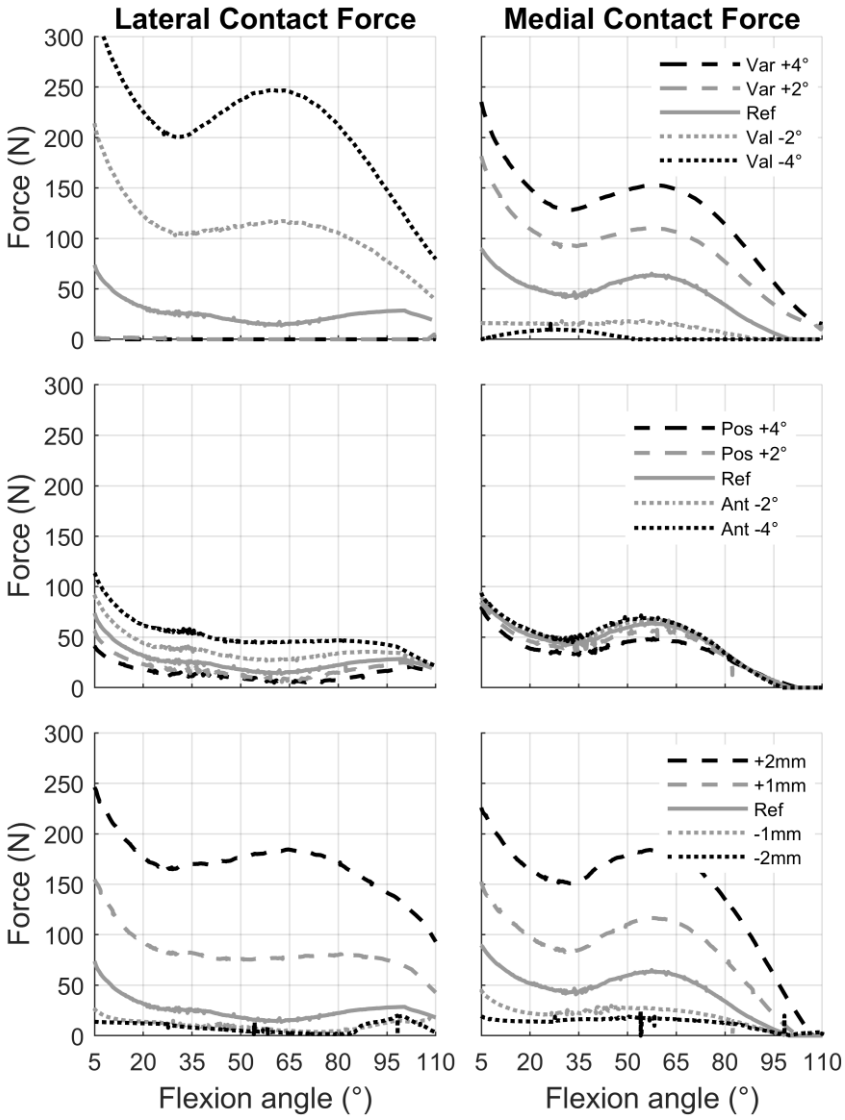

Figure 34. Impact of the tibial component varus/valgus tilt (top), anterior/posterior tilt (middle), and insert thickness (bottom) on the lateral and medial tibiofemoral contact forces.

3.2.5 Discussion

In this study, a computational multibody model of a prosthetic knee was implemented to investigate how the ligaments traction forces and tibiofemoral contact forces are affected when, starting from a balanced condition, the implant configuration is perturbed by varying the tibial tray slopes and insert thickness. In particular, the model behaviour was assessed throughout a simulated passive flexion motion.

First objective of this work consisted of obtaining a ligament balanced condition. Such reference condition was accomplished through an iterative ligament tuning process and evaluated on the basis of findings reported in other studies.

As far as concerning the resulting balanced model, over the whole flexion, all ligament bundles presented a maximum value below the threshold of 50 N suggested by Guess et al. (2017). Moreover, the bundles recruitment patterns were found to be consistent with what reported by (Blankevoort, Huiskes et al., 1991). The predicted tibiofemoral contact forces (maximum value of 163 N and maximum mediolateral difference of 52 N) are in agreement with other reported experimental measurements performed by means of sensing devices. For example, Asano and colleagues (H. Asano et al., 2004) reported a total contact force of 126.8 ± 23.6 N at knee extension. Looking separately to medial and lateral contact forces, Zapata et al. (Zapata et al., 2019) recorded average values of about 118 N and 85 N for the medial and lateral side, respectively. Overall, literature suggests contact forces within 90-180 N and a force difference between the medial

and lateral compartment lower than 67 N (H. Asano et al., 2004; Gustke et al., 2014; Verstraete et al., 2017; Walker et al., 2014). The contact forces trends, characterized by higher values in extension followed by a decrease with deeper flexion angles, confirmed what reported in other studies (Kebbach et al., 2019; Manning et al., 2019; Verstraete et al., 2017).

Results derived from implant variations revealed that, higher valgus slopes mostly affect the lateral ligament, which results clearly tougher than the medial one. On the other side, varus slopes produce the medial ligament tautening and, secondarily, a partial lateral loosening. As expected, the ligament force variations significantly affect the tibiofemoral contact forces. Indeed, valgus implant slopes also produce higher lateral contact force, whereas varus slopes produce higher medial contact force. In particular, the 4° valgus slop generated the highest measured contact force. Such result is meaningful since high unilateral contact forces can lead to intensified stresses of the polyethylene insert which, in turn, could increase the insert wearing.

The anterior/posterior implant variations produced the lowest variations in ligament tensioning and, consequently, also in contact forces. Specifically, higher anterior slopes lead to higher contact forces and vice versa. Such outcome is in accordance with the literature (Chen et al., 2015; Kebbach et al., 2019).

In contrast with the varus/valgus variation, which generate opposed force variations between medial and lateral compartments, variations of thickness as well as anterior/posterior slope symmetrically affect collateral ligaments and contact forces. However, in all cases, the ligament force

increase is followed by the widening of the ligament activation range, and vice versa.

Another aspect that deserves to be pointed out relays in the lift off phenomena (i.e. when the contact force becomes zero) since it causes joint instability. The medial lift off, which occurs after 100° in the balanced condition, could be due to an excessive initial valgus tibial slope, likely in combination with an anterior and/or proximal femoral component positioning (Verstraete et al., 2017). Moreover, results show that varus slopes represent the most critical changes since they lead to a complete lateral lift off over the whole flexion range. On the other hand, the increasing in valgus slopes leads to an early contact lost on the medial compartment.

In point of fact, the model developed in this study presents some limitations. Indeed, soft tissue structures surrounding the knee joint were simplified. In particular, being the ligaments modelled as straight-line elements, their wrapping around bony geometries was neglected, resulting in a slightly reduced ligament path length. This represents a good approximation in cases mainly involving knee flexion/extension movements. Conversely, results accuracy might be reduced when varus/valgus movements are investigated, since for such cases the force direction appears to move towards the center of the tibial plateau, crossing the bones condyles. In particular, in the presented study, such consideration concerns the MCL behaviour, especially during those configurations showing an increased varus slope of the tibial tray. In this regard, the presented model will be modified to investigate the impact of the ligament modelling on the obtained

results. In particular, each MCL bundle will be divided into consecutive 1D elements, so allowing the ligament wrapping of the joint.

Also, it should be noted that the absence of the extensor mechanism, and thus of the quadriceps passive resistance, may have led to underestimate the computed forces, although for a limited angles range at deep flexion. Nevertheless, the used ligament tuning method, showed its suitability in generating the ligament balancing needed as reference condition. Furthermore, the model has proven to be able to rapidly predict significant quantitative information in agreement with other experimental studies. In addition, the performed analysis highlights the high sensitivity of the ligament balancing to changes within 2 mm and 4° of insert thickness and tibial tray slope, respectively.

In conclusion, thanks to its computational efficiency (i.e. short simulation time), in combination with a furtherly improved software interface and possible sensing devices, the presented model would be intended as the first step toward the implementation of a valuable tool aimed to assisting the surgeon in preoperative or intraoperative evaluations of the ligaments balancing as well as the intra-articular contact forces during TKA.

Comparative Multibody Analysis of Ultra-congruent versus Medial-pivot Designs of Total Knee Arthroplasty*

To date, several configurations of TKA implants are commercially available whose designs came from clinical and biomechanical considerations. In particular, in the last two decades, research activities led to the development of increasingly sophisticated geometries including the so-called medial-pivot design, which aims to mimic the physiological internal/external tibial rotation (i.e., rotation around the tibial axis) that occurs during the knee flexion. Although most TKA show successful surgical outcomes, revision interventions are still carried out due to the onset of complications, such as joint instability and insert wear. These issues are related to several factors including the prosthesis design.

The present work investigates the impact of the insert design on the biomechanical behaviour of a TKA implant, comparing two different insert geometries, namely, the ultra-congruent (UC) and the medial-pivot (MP). In detail, the multibody model of a lower limb was created by assembling bone geometries with the TKA implant including the two alternative insert designs. In particular, the action of the quadriceps muscle group was integrated and computed through a PID controller. Moreover, the inserts geometry was discretized by means of a custom-made

*__Based on:__ Putame G, Terzini M, Rivera F, Bignardi C (2019) "Comparative analysis of ultra-congruent versus medial-pivot designs of total knee arthroplasty". *IX Annual Meeting of the Italian Chapter of the European Society of Biomechanics (ESB-ITA)*

macro, thus, the elastic foundation theory-based formulation was applied to estimate the contact parameters. The joint kinematics and dynamic were evaluated for each insert by simulating a deep squat motion. Furthermore, the contact pressure distribution on the inserts was investigated since this is an important determinant for the long-term implant success.

Results from kinematics and dynamics evaluations showed a similar tibial internal rotation range (about 3.5°) but different trends over the whole flexion motion. Indeed, an early rotation occurs for MP design with respect to the UC. No significant differences were found in total tibiofemoral contact force with a maximum value of 4.2 BW at 90° flexion. Conversely, from the contact pressure analysis, higher peak pressure resulted for UC design, underlining the essential role of the implant tibiofemoral conformity on both sagittal and frontal planes.

3.3.1 Background

Since the early 1970s, thanks to the collaboration between surgeons and bioengineers, increasingly sophisticated designs of TKA prosthesis have been developed (Ranawat and Ranawat, 2012). Among the several features that have to be taken into account during the implant design process there are, for instance, the range of motion, the modularity of the components, the type of insert fixation and, last but not least, the geometrical congruence between articulating surfaces (Dall'Oca et al., 2017). In particular, this last aspect represents a critical factor since tibiofemoral implant conformity must guarantee joint stability

and, at the same time, minimize contact force concentrations. In particular, the insert design assumes a major role in defining the artificial knee kinematics, which is related to wear performance and, consequently, to the longevity of the total knee replacement (Zhang et al., 2019). In fact, although the introduction of new materials and design concepts, complications related to joint instability and insert wear are still common causes of revision surgery (Navacchia et al., 2016). Focusing on the implant kinematics, since the late 1990s, the trend in implant design aimed to mimic the physiological medial-pivoting movement of the knee. Although, literature reports good surgical outcomes using the medial-pivot design (Atzori et al., 2016; Sabatini et al., 2018; Schmidt et al., 2003), it is unclear whether this design is significantly related to clinical and mechanical improvements with respect to traditional designs. Therefore, further investigations are needed in order to achieve a better understanding of the different implants' performance.

In this scenario, the possibility to predict *in vivo* kinematics and loading conditions of the artificial knee is essential to assess implant performance and improve the implant design as well as the surgical outcomes in total knee arthroplasty (TKA). Computational modelling can provide useful information about joint contact forces and kinematics in order to identify detrimental loading conditions that could lead to failure of the knee implant (Ardestani et al., 2015; Koh et al., 2019; Zhang et al., 2019). Specifically, musculoskeletal multibody models, characterized by a reduced complexity (e.g. considering a reduced group of muscles and/or neglecting some soft tissues of

the joint), have proven to be able to reproduce realistic kinematics and dynamic of the knee joint, besides to be particularly suitable for experimental validations (Bersini et al., 2016; Pianigiani et al., 2012; Twiggs et al., 2018; Zumbrunn et al., 2015).

In this study the biomechanical behaviour of two different insert designs, namely, the ultra-congruent (UC) and the medial-pivot (MP) was compared. For this reason, the multibody model of a lower limb was created by assembling bone geometries with the TKA implant including the two alternative insert designs. The kinematics and dynamic of the artificial knee were evaluated by simulating a weight-bearing deep squat motion. In particular, the contact force distribution on the inserts was investigated. In detail, the inserts geometry was discretized by means of a custom-made macro, thus, the elastic foundation theory-based formulation was applied to estimate the contact parameters at the tibiofemoral interface. Thanks to the discretization process, the contact locations as well as the pressure maps on the insert surface were also obtained within the multibody framework, therefore, without the need of further finite element analysis which, as known, imply intensive computational efforts. Initially, it was hypothesized that the MP design leads to higher internal/external tibial rotations and lower contact pressures with respect to the UC design.

3.3.2 Model

The multibody model of a right lower limb was created assembling standardized bone geometries (Sawbones® Europe AB, Malmoe, Sweden) with a TKA implant including two alternative insert designs, that are the ultra-congruent and medial-pivot.

Bone geometries were transformed in order to fit on patient-specific geometries available in literature (Fregly et al., 2012) corresponding to a male subject, who received a right knee prosthesis. More in detail, the center of the femoral head, the ankle midpoint, and the surgical cutting planes at the knee joint, were taken as spatial references during the fitting process of femoral and tibial bones (Figure 35a).

Moreover, the patella was represented by an ellipsoid, while the fibula was transformed in accordance to the tibia. In addition, scaled pelvis and foot bones were included as well.

Furthermore, the implant geometries were scaled, based on the manufacturer's sizes, in order to match the patient-specific bones. In details, the dual radius femoral component and both considered inserts were isotropically scaled up by a scale factor equal to 1.21, whereas the tibial tray was scaled up by a scale factor of 1.14, except for the normal direction to the component plateau which was not modified (Figure 35b).

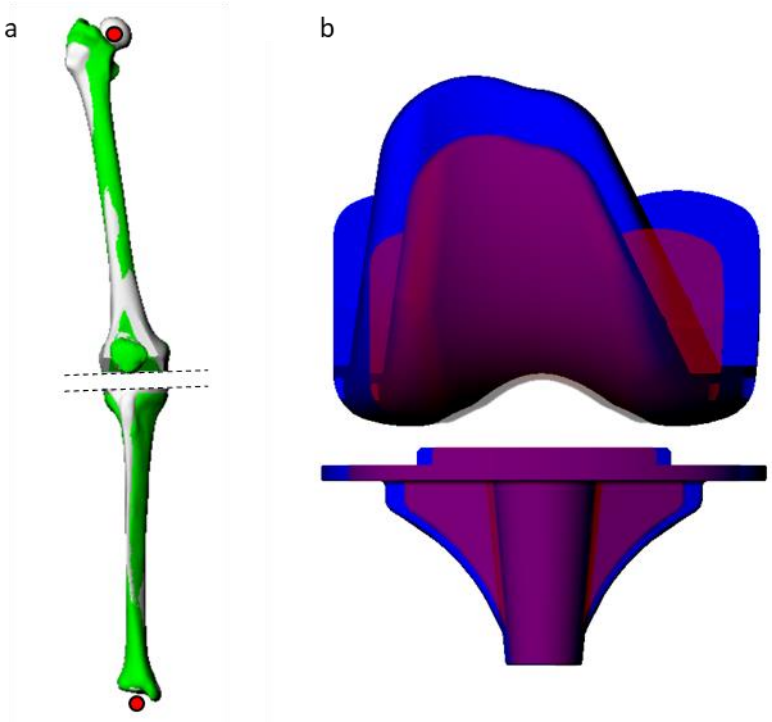

Figure 35. (**a**) Result of the fitting process between patient-specific (green) and standardized (grey) femoral and tibial bones. Red dots and dashed lines show the used spatial references; (**b**) Native (red) and scaled (blue) femoral and tibial components.

Furthermore, the following ligaments were included in the model: medial (MCL) and lateral (LCL) collateral ligaments, medial (MFPL) and lateral (LFPL) patellofemoral ligaments, and patellar ligament (PL). Anterior and posterior cruciate ligaments were not included since they are often sacrificed during the TKA surgical procedure. Each ligaments was furtherly split into different bundles, in detail: MCL anterior (aMCL), intermediate (iMCL) and posterior (pMCL) bundle; LCL anterior (aLCL) and

posterior (pLCL) bundle; LFPL proximal (pLFPL), middle (mLFPL) and distal (dLFPL) bundle; MFPL proximal (pMFPL), middle (mMFPL) and distal (dMFPL) bundle; PL medial (mPL), intermediate (iPL) and lateral (lPL). This division allows considering the ligament structure in bundles with their different constraining contribution. In Figure 36 shows the attachment points and orientations of each ligament bundle. Origin and insertion points were determined from anatomical references. Table 7 lists all considered ligaments bundles with the related stiffness parameters *k*, which were retrieved from literature (Bersini et al., 2016; Guess and Razu, 2017; Marra et al., 2015; Piazza and Delp, 2001).

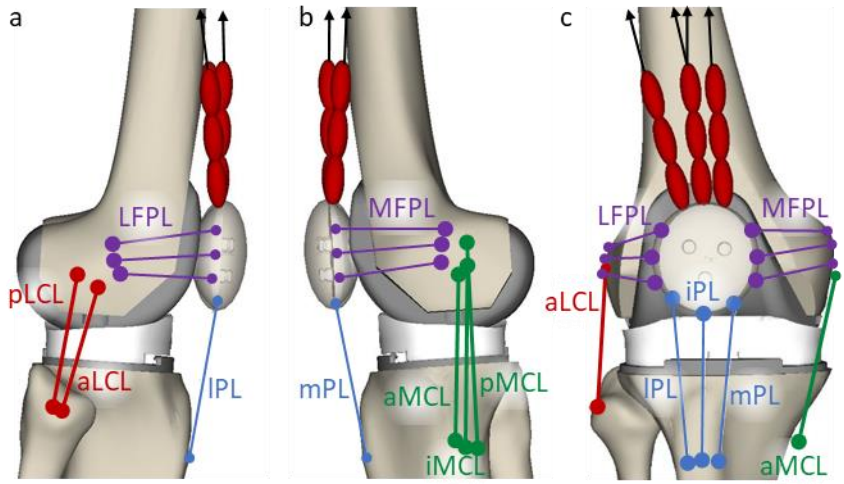

Figure 36. Ligament bundles included into the model. (**a**) Lateral view; (**b**) medial view; (**c**) frontal view. Red ellipsoids represent quadriceps tendons and black upward arrows indicate muscles directions.

Table 7. Stiffness parameters (expressed as force per unit strain) for each ligament bundle.

Ligament bundle	*k (N)*
aMCL	2500 [1]
iMCL	3000 [1]
pMCL	2500 [1]
aLCL	2000 [1,2]
pLCL	2000 [1,2]
lPL	58000 [3]
iPL	58000 [3]
mPL	58000 [3]
pMPFL	141 [4]
mMPFL	141 [4]
dMPFL	141 [4]
pLPFL	141 [4]
mLPFL	141 [4]
dLPFL	141 [4]

From [1]Bersini et al. (2015), [2]Marra et al. (2015), [3]Piazza et al. (2001), [4]Guess et al. (2017).

The zero-load length of each ligament bundle was tuned by iteratively performing the simulation of a passive knee flexion (see paragraph 3.2.2.1) and simultaneously adjusting the ligament zero-load lengths by steps of 1% with respect to the initial values. Furthermore, as necessary, the attachment points of the bundles were also adjusted to agree with the reported recruitment patterns of the bundles (Blankevoort, Huiskes et al., 1991).

The quadriceps muscle group was also implemented into the model. In particular, the vastus medialis (Vmed), vastus intermedius (Vint), vastus lateralis (Vlat) and rectus femoris (RF) were considered as distinct traction forces. Origin and insertion muscles points were adapted from data reported in literature

(Delp et al., 1990). Proximally, all muscles origin from the femur diaphysis, except for the rectus femoris, which arises from the anterior inferior iliac spine (Figure 37). Distally, muscles insert on the upper edge of the patella through tendons that are modelled as chained ellipsoids. Such tendons representation is important to allow the femoral wrapping mechanism that occurs during the knee flexion. Muscles forces were obtained by means of a PID controller. To take into account the different muscle contribution, the controller output force was multiplied by the specific physiological cross-sectional area (Table 8) normalized by the mean PCSA (2147 mm2). Moreover, each muscle force was limited within a physiological range (see paragraph 2.4). After the controller tuning process, the proportional, integrative and derivative K gains resulted equal to 300, 5 and 3, respectively.

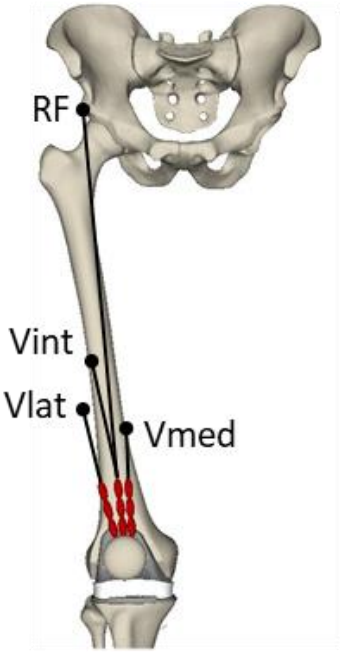

Figure 37. Muscles included into the model: Vastus medialis (Vmed), Vastus lateralis (Vlat), Vastus intermedius (Vint), Rectus femoris (RF).

Table 8. Muscles included into the model with relative PCSAs

Muscle	*PCSA (mm^2)*
Vastus medialis	2060
Vastus intermedius	1670
Vastus lateralis	3510
Rectus femoris	1350

From Ward et al. (2009)

In order to predict the tibiofemoral pressure distribution, both considered insert geometries were discretized into hexahedral elements with a cross-sectional area of 4 mm^2 (Figure 38). Thereby, the elastic foundation theory-based formulation was used to define the contact between the femoral component and each insert element. In particular, the contact stiffness was computed using the Equation 6, considering E = 648 MPa, ν = 0.46 (Zaribaf, 2018) and h = 10 mm. Then, contact parameters were tuned based on the method describe before (see paragraph 2.3.3). Furthermore, to reduce high-frequency noise, the resulting contact forces were filtered by means of a zero-phase Butterworth low-pass filter (order 2, cut-off frequency 5 Hz).

Two additional contact pairs were also defined, between the femoral and patellar component and between the femoral component and each quadriceps tendon element, using the Hertz's law-based formulation. Friction forces between implant components were considered considering values of 0.03 and 0.01 as static and dynamic friction coefficient, respectively (Stylianou et al., 2013). Table 9 summarizes the values used for contacts implementation.

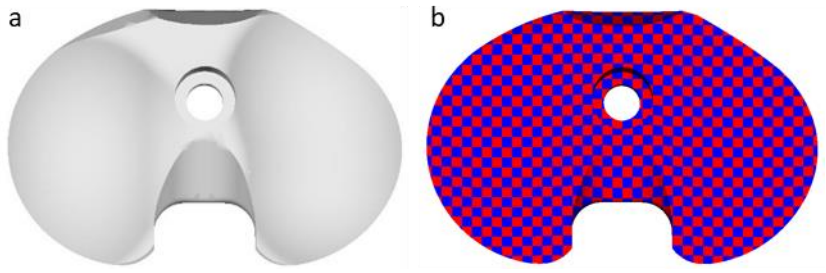

Figure 38. Illustrative result of the discretization process applied to the medial-pivot inserts. Upper view of the (**a**) native and (**b**) discretized geometry.

Table 9. Value of contact stiffness (K), the nonlinear power exponent (e), maximum damping constant (C_{max}), maximum penetration constant (δ_{max}) for the different contact pairs.

Contact pair	*K* *(N/mm^e)*	*C_{max}* *(Ns/mm)*	*δ_{max}* *(mm)*	*e*
Femoral component Insert element	1198	375	0.1	1.0
Femoral component Patellar component	30000	60	0.1	1.5
Femoral component Quadriceps tendon	500	5	0.1	2.0

As regards the mass properties of the bodies, a density of 4850 kg/m^3 and 930 kg/m^3 was assigned to each implant metal component and the polyethylene insert, respectively. Also, a density of 2680 kg/m^3 was assigned for tendons (Hashemi et al., 2005). Moreover, an average density of 1600 kg/m^3 was assumed for the femur, whereas a value of 2740 kg/m^3 was used for the patella, fibula and tibia (Guess et al., 2010). In addition, a mass fraction of 29.3 kg was assigned to the pelvis. Such mass fraction

was derived through the sum of the body segments weights (head, neck, upper arm, forearm, hand, trunk and thigh) computed as percentage of the whole-body weight (Tözeren, 2000) for a male subject of 66.7 kg.

3.3.2.1 Insert Designs

The two considered knee implants are characterized by identical femoral and tibial components, but fixed-bearing inserts with different geometries.

Overall, the medial-pivot (MP) insert (Figure 39a) is characterized by a reduced lateral congruence with respect to the medial one. The purpose of this asymmetry is to replicate the physiological tibiofemoral kinematics that involves the tibial internal rotation during knee flexion.

Conversely, the ultra-congruent (UC) insert (Figure 39b) should guarantee a high congruence between femoral and insert surfaces, over the whole flexion range, having a symmetric shape with respect to the sagittal plane.

However, comparing the sagittal section of each compartment between the inserts (Figure 40), it is possible to see that, on the medial side, the MP presents a more congruent compartment than the UC, whereas, on the lateral side, the MP compartment shows a significantly lower anterior edge as well as a slightly higher posterior edge with a smaller radius of curvature and, above all, a flat profile at the middle of the compartment. Looking at the insert section on the frontal plane, it can be seen that both compartments of the MP present a slightly smaller radius of curvature than the UC.

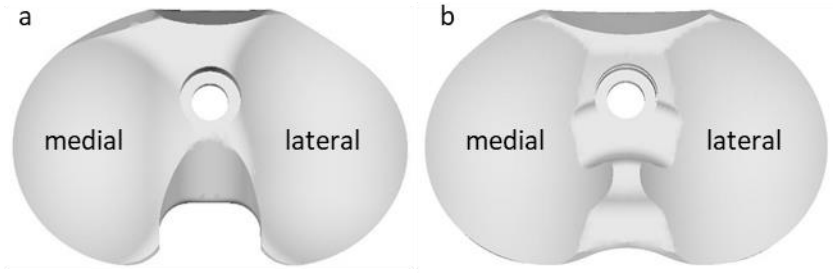

Figure 39. Insert designs: (**a**) Medial-pivot versus (**b**) ultra-congruent.

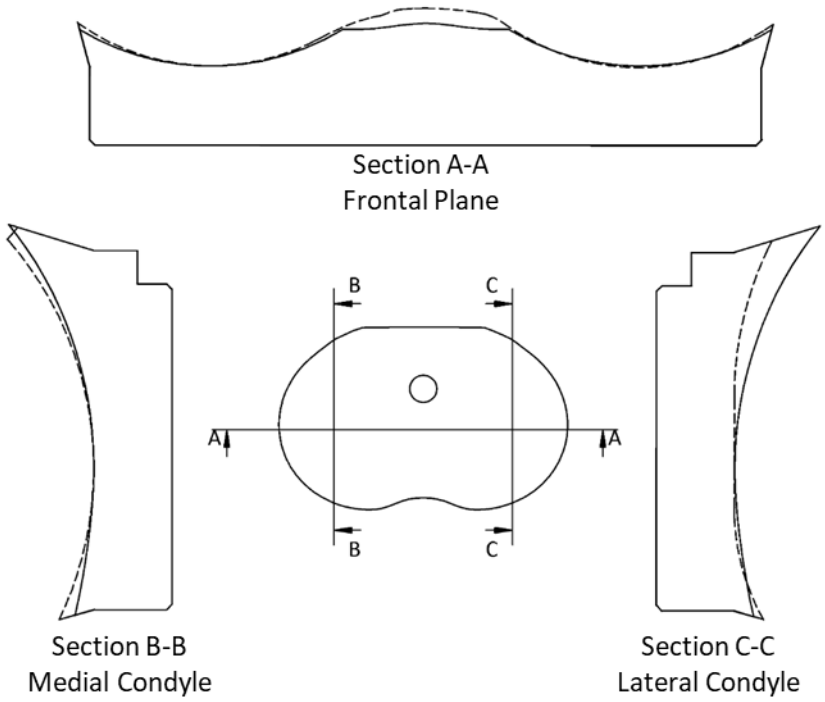

Figure 40. Comparison between the medial-pivot (dashed profiles) and ultra-congruent (solid lines) designs.

3.3.2.2 Squat Simulation

In order to compare the dynamics and kinematics behaviour produced by the different insert designs, a weight-bearing squat simulation was performed including the gravitational field. During the squat, the pelvis was constrained to translate along the vertical direction (Figure 41a), while only the flexion movement was allowed at the hip joint. All six degrees of freedom were permitted at the patella. Moreover, the tibia was constrained to the foot through the ankle joint which was defined to prevent vertical and anteroposterior relative translations (Tanaka et al., 2016). Finally, the foot was fixed on the ground (i.e., foot-ground contact has not been implemented).

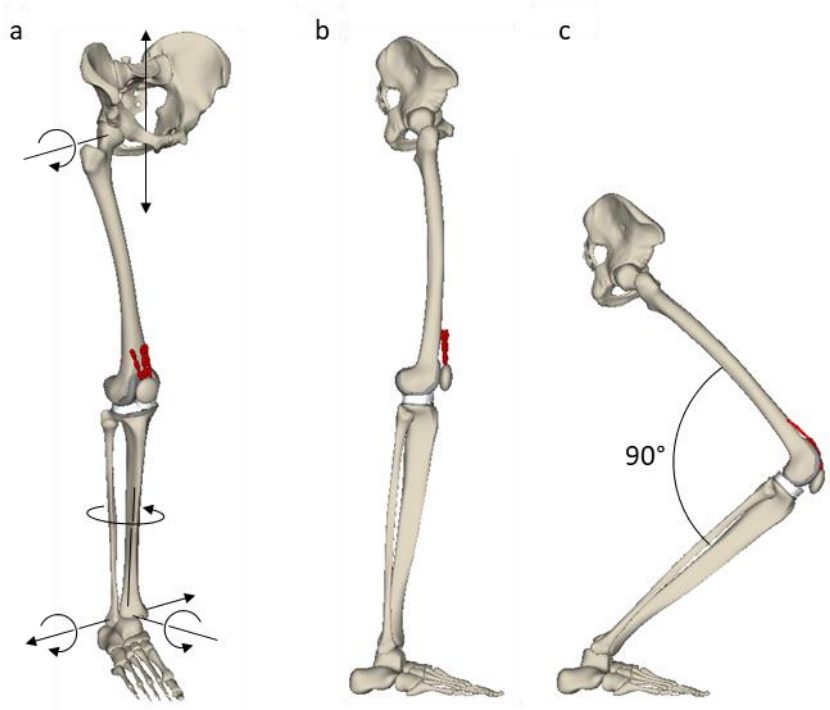

Figure 41. (**a**) Multibody model of the right leg with black arrows indicating the d.o.f. assigned to the pelvis, hip, and ankle during the squat simulation; (**b**) lateral view of the model in full extension and (**c**) 90° flexion.

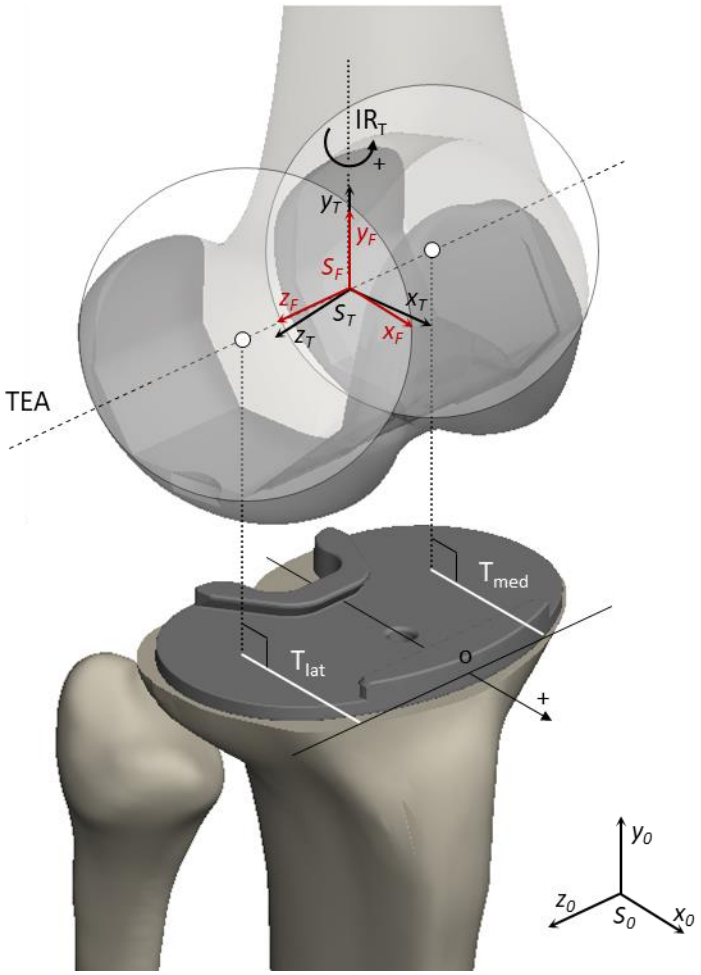

Figure 42. Defined references to measure the tibial internal rotation (IR_T) and the anteroposterior translation of each condyle. It can be seen the transepicondylar axis (TEA) passing through the centers (white points) of two spheres inscribing the femoral condyles. Also, the two body-fixed reference systems for the femur (S_F in red) and the tibia (S_T in black) are showed. These are located on the TEA in the middle of the centers of the spheres and used to measure the IR_T as the relative rotation of S_T with respect to S_F along the *y* direction. At the beginning of the simulation S_F and S_T are coincident with the y axis along the y_0 axis of the global reference system (S_0). The anteroposterior positions of both lateral (T_{lat}) and medial (T_{med}) condyle are obtained as the projection (white lines) on the tibial tray of the minimal distance between the center of the spheres and the anterior edge of the tibial tray. The condyle position is measured along an axis pointing anteriorly and having origin at the anterior edge of the tibial tray (point O). Therefore, measured positions result negatives.

The knee flexion was achieved by defining a specific vertical displacement for the femoral head center, hence, the implemented PID controller continuously adjusted the quadriceps muscle forces to follow the target displacement, generating a knee flexion from extension to 90° flexion in approximately 2.2 s (Figure 41b-c).

As regards kinematics measurements, tibial internal rotation was derived from the relative angular displacements between two defined body-fixed reference systems, one for the femur and the other for the tibia (Figure 42), both with same orientation and located along the transepicondylar axis (TEA), which is defined as the line passing through the centers of two spheres inscribing the femoral condyles (T. Asano et al., 2001), in the middle of the centers of the spheres. Therefore, the anteroposterior position of each condyle was measured as the projection on the tibial tray of the minimal distance between the center of the sphere inscribing the condyle and the anterior edge of the tibial component. Based on the so defined references, the anteroposterior translation value increases negatively when the femoral condyle moves posteriorly.

3.3.3 Results

Results from squat simulations, involving the two alternative insert designs, were compared in terms of: tibiofemoral contact force, pressure distribution on the insert surface, anteroposterior translation (femoral rollback) of the lateral and medial femoral condyles, and tibial internal rotation.

First, kinematics results showed similar ranges of internal tibial rotation for the MP and UC insert, that is, 3.5° and 3.4°,

respectively (Figure 43). However, it is possible to note a different trend over the whole flexion. Indeed, the UC design generates almost no rotation over the first 30°, maintaining a constant value of about 0°, then the rotation increases linearly up to 3.3°. Conversely, the MP design shows an early increase, reaching 3° of internal rotation at about 45° flexion, successively the rotation stays within a range of 3-4°.

Overall, femoral rollback measurements show an anterior translation, over the first 35°, followed by a more or less pronounced posterior translation (Figure 44). In detail, both designs generate a medial anterior translation of 4.4 mm, whereas the lateral anterior translation results equal to 3.9 mm for the UC and only 2.3 mm for the MP. From about 35° flexion onwards, in both designs, the lateral femoral condyle performs a rollback that recovers the previous anterior translation. On the other side, the medial rollback is limited to 1.1 mm and 1.8 mm for the UC and MP, respectively.

As concerning measured tibiofemoral contact forces (Figure 45), values equal to 561 N and 609 N were obtained in extension for the UC and MP, respectively. Then, for both designs, the contact force increases over the whole knee flexion leading to a maximum common value of about 2824 N at 90° flexion, which corresponds to 4.2 times the total body weight (BW).

Although no significant differences between UC and MP insert were observed in total tibiofemoral contact forces, the relative contact pressure distributions on the tibial surface revealed important distinctions.

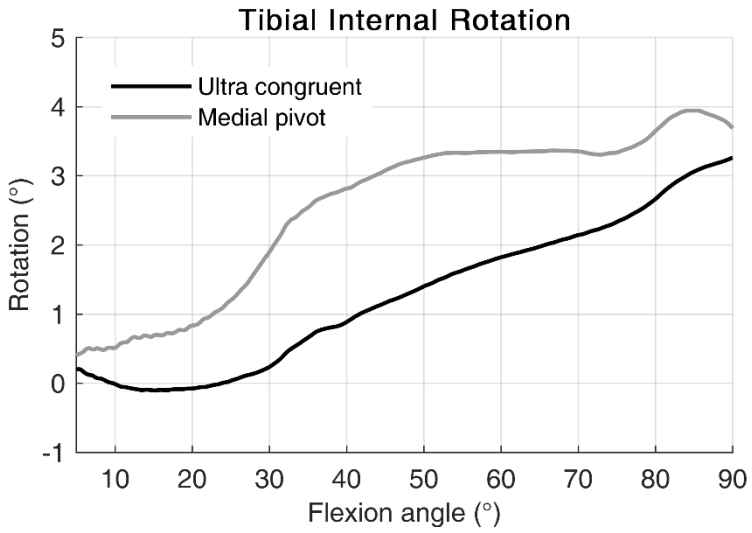

Figure 43. Tibial internal rotation during the squat movement.

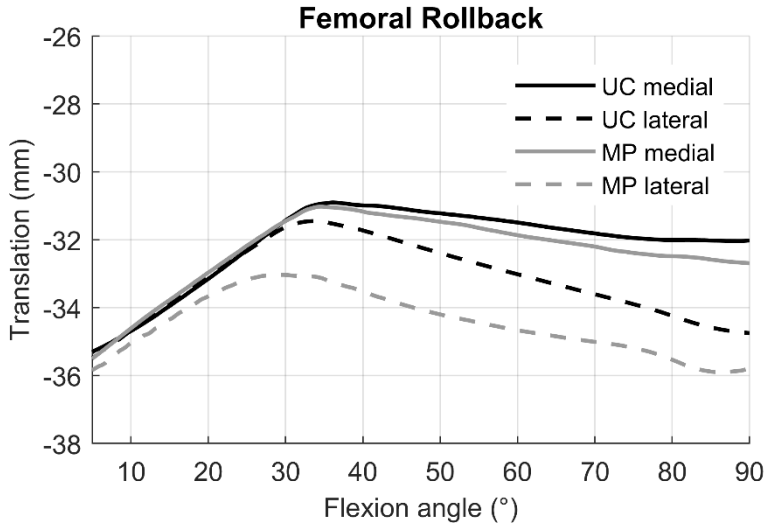

Figure 44. Medial and lateral femoral condyles rollback during the squat movement for both medial-pivot (MP) and ultra-congruent (UC) inserts.

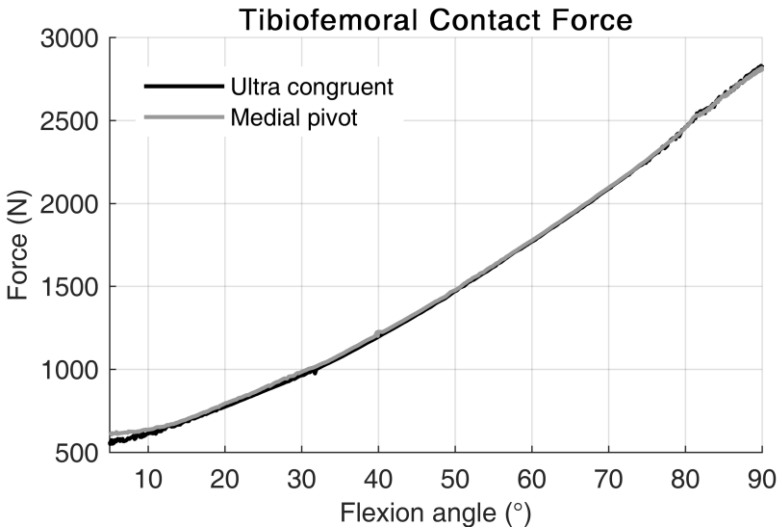

Figure 45. Total tibiofemoral contact force during the squat movement.

Overall, contact pressures increase together with the flexion angle, reaching the highest values at 90° flexion (Figure 46). Nevertheless, it is clear that the UC design causes more concentrated contact forces than the MP design, on both medial and lateral insert compartments. Specifically, the UC design presents narrower and more rounded contact footprints, whereas the MP design is characterized by wider contact footprints. In particular, the MP design presents a well distributed contact on the medial compartment for 10° flexion. Peak pressures resulted equal to 20 MPa and 33 MPa for MP and UC design, respectively. Such peak values were found on the medial side in both designs. Furthermore, it is possible to note that the lateral contact moves posteriorly, in contrast with the medial one which moves slightly anteriorly over the flexion.

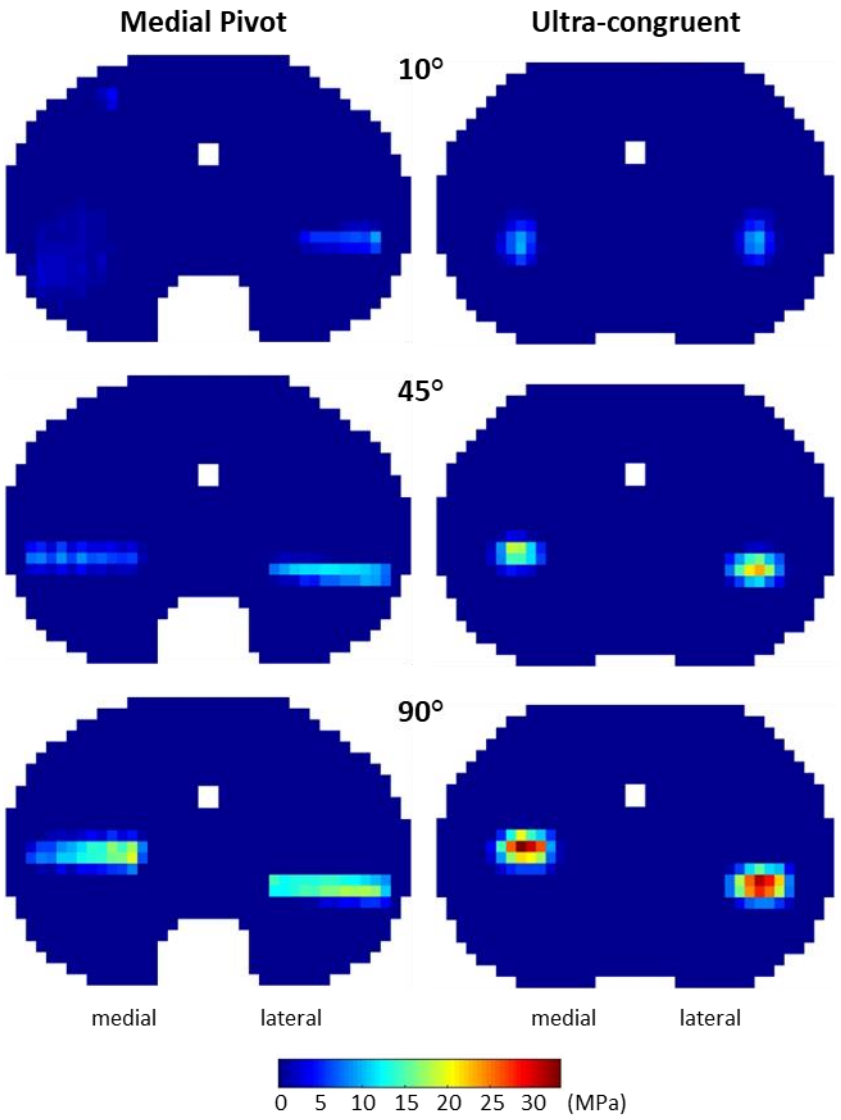

Figure 46. Pressure distribution on the insert surface at three successive flexion angles (10°, 45° and 90°) during the squat movement.

3.3.4 Discussion

The present study investigates two different insert designs for total knee arthroplasty. A multibody model of the right lower limb was created and scaled on patient-specific bones including the prosthetic knee derived from two alternative insert geometries, that is, medial-pivot and ultra-congruent. For the two resulting models, dynamics and kinematics behaviours were evaluated during a squat movement task. In particular, the following quantities were computed and compared: tibiofemoral contact force, pressure distribution on the insert surface, anteroposterior translation (femoral rollback) of the lateral and medial femoral condyles, and tibial internal rotation.

In contrast with what initially hypothesized, both insert designs show similar ranges of internal tibial rotation. However, kinematics results revealed that the inserts generate a different trend of the tibial internal rotation. Especially, over the first 30° of flexion, the MP design showed a more physiological behaviour allowing for the internal rotation, while the UC design seems to hinder the rotation in the same flexion range. This difference appears particularly significant considering that, during level walking in one gait cycle, the knee flexion angle stays below 30° throughout the stance phase and the second part of the swing phase (i.e. compressively about 70% of the gait cycle).

From femoral rollback measurements, during the first 35° of flexion, it can be noted the so-called “paradoxical motion”, that is the anterior translation of the femoral condyles. Such anterior femoral sliding, although being not physiological, was observed

in most of the TKA designs and should be carefully considered since it may lead to patient dissatisfaction (Dennis et al., 2003; Sabatini et al., 2018).

From results concerning the total contact forces, no significant differences arose. However, in extension, the MP design generate a higher force (+8.5%) than the UC. This difference may be due to a greater restraining effect exerted by the medial compartment of the MP design. The maximum contact force of 4.2 BW is within the range of 2.3-7.3 BW reported in literature (Mizu-uchi et al., 2015).

The contact pressure distributions acting on the tibial component highlight that, if compared to the MP geometry, the UC geometry causes force concentrations which could trigger or speed up wearing phenomena. This is probably due to the greater radius of curvature of the medial and lateral compartments that the UC design presents on the frontal plane. Indeed, even if minimal, such difference produces a lower conformity on the sagittal plane between the femoral condyles and UC insert compartments, explaining the more rounded shape of the contact footprints. Conversely, the higher conformity of the MP design on the frontal plane, justifies the wider contact footprints extended along the mediolateral axis. The maximum pressure values obtained in this work (20 MPa and 33 MPa for MP and UC design, respectively), are consistent with other numerical studies. For instance, Bei and Fregly (2004) reported a peak pressure of 28 MPa, during a gait cycle, under a load of 3 BW. In their experiments, Fregly et al. (2003) measured peaks pressure between 25 and 35 MPa, under a loading condition of 3000 N at

90° flexion. Furthermore, Stylianou et al. (2013) predicted a maximum value of about 26 MPa, during a squat motion when at 2500 N of tibiofemoral compressive force. However, it has to be stated that direct comparisons with other studies should be carefully interpreted since findings are highly design-dependent, especially those relative to the contact pressure.

This study presents some limitations that need to be pointed out. First, ligaments locations were derived by anatomical references. A better approach would be to derive the ligaments attachment points directly from MRI images. Second, although in line with other reported analysis, only the quadriceps muscle group was implemented. In future developments, additional muscle will be integrated into the model (e.g. the hamstrings). Furthermore, the performed weight-bearing squat simulation with the specifically set constraints, does not exactly mimic a real squat movement. This latter could be obtained by integrating experimentally kinematics data into the model. On the other hand, the implemented squat simulation allows for realistic knee loading conditions and is particularly suitable for being validated *in vitro* by means of experimental setups, i.e. test rigs.

Finally, it should be stated that findings were not directly validated against *ad hoc* experiments, however a comparison with reported data was performed showing good agreements with the literature.

In conclusion, the presented multibody comparative analysis, allowed for a realistic investigation of the TKA performance, which is essential for the implant design developments and optimizations. Moreover, the integration of the discretization

process applied to the insert geometry, confirmed that additional significant outcomes can be efficiently obtained directly within the multibody framework.

Conclusions

Computational multibody modelling has been proven to be a powerful tool whether applied for biomechanical investigations.

In this thesis, a series of modelling strategies were properly exploited with the objective to improve the understanding of specific orthopaedic issues related to the biomechanical behaviour of the anatomical and artificial knee joint in canine and human subjects, respectively.

The described methodologies enabled to assess the effectiveness of two alternative tibial osteotomies used for treatment of canine anterior cruciate ligament rupture, highlighting both advantages and disadvantages of each surgical procedure.

Furthermore, in combination with a purposely implemented interactive software interface, the creation of a human knee model, undergone to total arthroplasty, allowed for the evaluation of the collateral ligament tensions and tibiofemoral contact forces during a passive knee flexion, underlining the sensitivity of these

quantities to different variations in the implant alignment and insert thickness.

Finally, the development of a human lower limb model permitted a comparative analysis between two alternative insert designs for total knee arthroplasty. Specifically, the presented findings revealed the critical impact of both frontal and sagittal tibiofemoral conformity in reducing contact pressure distributions on the insert surface.

More in general, this study confirms the great potential of the computational multibody approach in assisting the surgeon in preoperative or intraoperative evaluations.

References

Aglietti, P., and Menchetti, P. P. M. (1995). Biomechanics of the Patellofemoral Joint. In G. R. Scuderi (Ed.), *The Patella* (pp. 25–48). Springer New York. https://doi.org/10.1007/978-1-4612-4188-1_3

An, K. N., Kaufman, K. R., and Chao, E. Y. S. (1989). Physiological considerations of muscle force through the elbow joint. *Journal of Biomechanics*, *22*(11–12), 1249–1256. https://doi.org/10.1016/0021-9290(89)90227-3

Ardestani, M. M., Moazen, M., and Jin, Z. (2015). Contribution of geometric design parameters to knee implant performance: Conflicting impact of conformity on kinematics and contact mechanics. *Knee*, *22*(3), 217–224. https://doi.org/10.1016/j.knee.2015.02.011

Armand, M., Grupp, R., Murphy, R., Hegman, R., Armiger, R., Taylor, R., McArthur, B., and Lepisto, J. (2018). Biomechanical guidance system for periacetabular osteotomy. In G. Zheng, W. Tian & X. Zhuang (Eds.), *Advances in Experimental Medicine and Biology* (Vol. 1093, pp. 169–179). Springer Singapore. https://doi.org/10.1007/978-981-13-1396-7_14

Asano, H., Hoshino, A., and Wilton, T. J. (2004). Soft-tissue tension total knee arthroplasty. *The Journal of Arthroplasty*, *19*(5), 558–561. https://doi.org/10.1016/j.arth.2004.01.003

Asano, T., Akagi, M., Tanaka, K., Tamura, J., and Nakamura, T. (2001). In Vivo Three-Dimensional Knee Kinematics Using a Biplanar Image-Matching Technique. *Clinical*

Orthopaedics and Related Research, *388*(388), 157–166. https://doi.org/10.1097/00003086-200107000-00023

Atzori, F., Salama, W., Sabatini, L., Mousa, S., and Khalefa, A. (2016). Medial pivot knee in primary total knee arthroplasty. *Annals of Translational Medicine*, *4*(1), 4–7. https://doi.org/10.3978/j.issn.2305-5839.2015.12.20

Beer, P., Bockstahler, B., and Schnabl-Feichter, E. (2018). Tibial plateau leveling osteotomy and tibial tuberosity advancement - A systematic review. *Tierarztliche Praxis Ausgabe K: Kleintiere - Heimtiere*, *46*(4), 223–235. https://doi.org/10.15654/TPK-170486

Bei, Y., and Fregly, B. J. (2004). Multibody dynamic simulation of knee contact mechanics. *Medical Engineering and Physics*, *26*(9 SPEC.ISS.), 777–789. https://doi.org/10.1016/j.medengphy.2004.07.004

Bersini, S., Sansone, V., and Frigo, C. A. (2016). A dynamic multibody model of the physiological knee to predict internal loads during movement in gravitational field. *Computer Methods in Biomechanics and Biomedical Engineering*, *19*(5), 571–579. https://doi.org/10.1080/10255842.2015.1051972

Bertocci, G. E., Brown, N. P., Embleton, N. A., and Barkowski, V. J. (2016). Canine Stifle Biomechanics Associated With a Novel Extracapsular Articulating Implant Predicted Using a Computer Model. *Veterinary Surgery*, *45*(3), 327–335. https://doi.org/10.1111/vsu.12450

Blackburn, T. A., and Craig, E. (1980). Knee Anatomy. *Physical Therapy*, *60*(12), 1556–1560.

https://doi.org/10.1093/ptj/60.12.1556

Blankevoort, L., Huiskes, R., and de Lange, A. (1991). Recruitment of Knee Joint Ligaments. *Journal of Biomechanical Engineering*, *113*(1), 94. https://doi.org/10.1115/1.2894090

Blankevoort, L., Kuiper, J. H., Huiskes, R., and Grootenboer, H. J. (1991). Articular contact in a three-dimensional model of the knee. *Journal of Biomechanics*, *24*(11), 1019–1031. https://doi.org/10.1016/0021-9290(91)90019-J

Boero Baroncelli, A., Reif, U., Bignardi, C., and Peirone, B. (2013). Effect of Screw Insertion Torque on Push-Out and Cantilever Bending Properties of Five Different Angle-Stable Systems. *Veterinary Surgery*, *42*(3), 308–315. https://doi.org/10.1111/j.1532-950X.2013.01088.x

Boudrieau, R. J. (2009). Tibial Plateau Leveling Osteotomy or Tibial Tuberosity Advancement? *Veterinary Surgery*, *38*(1), 1–22. https://doi.org/10.1111/j.1532-950X.2008.00439.x

Brown, N. P., Bertocci, G. E., and Marcellin-Little, D. J. (2013). Development of a Canine Stifle Computer Model To Evaluate Cranial Cruciate Ligament Deficiency. *Journal of Mechanics in Medicine and Biology*, *13*(02), 1350043. https://doi.org/10.1142/s0219519413500437

Carpenter, D. H., and Cooper, R. C. (2000). Mini review of canine stifle joint anatomy. *Anatomia Histologia Embryologia*, *29*(6), 321–329. https://doi.org/10.1046/j.1439-0264.2000.00289.x

Chen, Z., Wang, L., Liu, Y., He, J., Lian, Q., Li, D., and Jin, Z. (2015). Effect of component mal-rotation on knee loading in

total knee arthroplasty using multi-body dynamics modeling under a simulated walking gait. *Journal of Orthopaedic Research*, *33*(9), 1287–1296. https://doi.org/10.1002/jor.22908

Chen, Z., Zhang, X., Ardestani, M. M., Wang, L., Liu, Y., Lian, Q., He, J., Li, D., and Jin, Z. (2014). Prediction of in vivo joint mechanics of an artificial knee implant using rigid multi-body dynamics with elastic contacts. *Proceedings of the Institution of Mechanical Engineers, Part H: Journal of Engineering in Medicine*, *228*(6), 564–575. https://doi.org/10.1177/0954411914537476

Cho, K. J., Seon, J. K., Jang, W. Y., Park, C. G., and Song, E. K. (2018). Objective quantification of ligament balancing using VERASENSE in measured resection and modified gap balance total knee arthroplasty. *BMC Musculoskeletal Disorders*, *19*(1), 1–11. https://doi.org/10.1186/s12891-018-2190-8

Dall'Oca, C., Ricci, M., Vecchini, E., Giannini, N., Lamberti, D., Tromponi, C., and Magnan, B. (2017). Evolution of TKA design. *Acta Biomedica*, *88*(2-S), 17–31. https://doi.org/10.23750/abm.v88i2-S.6508

Delp, S. L., Loan, J. P., Hoy, M. G., Zajac, F. E., Topp, E. L., and Rosen, J. M. (1990). An interactive graphics-based model of the lower extremity to study orthopaedic surgical procedures. *IEEE Transactions on Biomedical Engineering*, *37*(8), 757–767. https://doi.org/10.1109/10.102791

Dennis, D. A., Komistek, R. D., Mahfouz, M. R., Haas, B. D., and Stiehl, J. B. (2003). Conventry Award Paper:

Multicenter Determination of In Vivo Kinematics After Total Knee Arthroplasty. *Clinical Orthopaedics and Related Research*, *416*(416), 37–57. https://doi.org/10.1097/01.blo.0000092986.12414.b5

Drew, J. O., Glyde, M. R., Hosgood, G. L., and Hayes, A. J. (2018). The Effect of Tibial Plateau Levelling Osteotomy on Stifle Extensor Mechanism Load: A Canine Ex Vivo Study. *Veterinary and Comparative Orthopaedics and Traumatology*, *31*(2), 131–136. https://doi.org/10.1055/s-0038-1627476

Fitzpatrick, C. K., Baldwin, M. A., Clary, C. W., Maletsky, L. P., and Rullkoetter, P. J. (2012). Evaluating knee replacement mechanics during ADL with PID-controlled dynamic finite element analysis. *Computer Methods in Biomechanics and Biomedical Engineering*, *17*(4), 360–369. https://doi.org/10.1080/10255842.2012.684242

Flores, P. (2011). Compliant contact force approach for forward dynamic modeling and analysis of biomechanical systems. *Procedia IUTAM*, *2*, 58–67. https://doi.org/10.1016/j.piutam.2011.04.006

Flores, P., Flores, P., and Lankarani, H. M. (2016). *Solid Mechanics and Its Applications Contact Force Models for Multibody Dynamics* (Issue April).

Fregly, B. J., Bei, Y., and Sylvester, M. E. (2003). Experimental evaluation of an elastic foundation model to predict contact pressures in knee replacements. *Journal of Biomechanics*, *36*(11), 1659–1668. https://doi.org/10.1016/S0021-9290(03)00176-3

Fregly, B. J., Besier, T. F., Lloyd, D. G., Delp, S. L., Banks, S. A., Pandy, M. G., and D'Lima, D. D. (2012). Grand challenge competition to predict in vivo knee loads. *Journal of Orthopaedic Research*, *30*(4), 503–513. https://doi.org/10.1002/jor.22023

Galbusera, F., Freutel, M., Dürselen, L., D'Aiuto, M., Croce, D., Villa, T., Sansone, V., and Innocenti, B. (2014). Material Models and Properties in the Finite Element Analysis of Knee Ligaments: A Literature Review. *Frontiers in Bioengineering and Biotechnology*, *2*(November), 1–11. https://doi.org/10.3389/fbioe.2014.00054

Geier, A., Kluess, D., Grawe, R., Herrmann, S., D'Lima, D., Woernle, C., and Bader, R. (2017). Dynamical analysis of dislocation-associated factors in total hip replacements by hardware-in-the-loop simulation. *Journal of Orthopaedic Research*, *35*(11), 2557–2566. https://doi.org/10.1002/jor.23549

Goldblatt, J. P., and Richmond, J. C. (2003). Anatomy and biomechanics of the knee. *Operative Techniques in Sports Medicine*, *11*(3), 172–186. https://doi.org/10.1053/otsm.2003.35911

Grelsamer, R. P., and Klein, J. R. (1998). The Biomechanics of the Patellofemoral Joint. *Journal of Orthopaedic & Sports Physical Therapy*, *28*(5), 286–298. https://doi.org/10.2519/jospt.1998.28.5.286

Grosu, S., Cherelle, P., Verheul, C., Vanderborght, B., and Lefeber, D. (2014). Case study on human walking during wearing a powered prosthetic device: Effectiveness of the

system “human-Robot.” *Advances in Mechanical Engineering*, *2014*. https://doi.org/10.1155/2014/365265

Guess, T. M., and Razu, S. (2017). Loading of the medial meniscus in the ACL deficient knee: A multibody computational study. *Medical Engineering & Physics*, *41*(3), 26–34. https://doi.org/10.1016/j.medengphy.2016.12.006

Guess, T. M., Razu, S., and Jahandar, H. (2016). Evaluation of Knee Ligament Mechanics Using Computational Models. *The Journal of Knee Surgery*, *29*(2), 126–137. https://doi.org/10.1055/s-0036-1571954

Guess, T. M., Stylianou, A. P., and Kia, M. (2014). Concurrent prediction of muscle and tibiofemoral contact forces during treadmill gait. *Journal of Biomechanical Engineering*, *136*(2). https://doi.org/10.1115/1.4026359

Guess, T. M., Thiagarajan, G., Kia, M., and Mishra, M. (2010). A subject specific multibody model of the knee with menisci. *Medical Engineering and Physics*, *32*(5), 505–515. https://doi.org/10.1016/j.medengphy.2010.02.020

Gustke, K. A., Golladay, G. J., Roche, M. W., Elson, L. C., and Anderson, C. R. (2014). A new method for defining balance: Promising Short-Term Clinical Outcomes of Sensor-Guided TKA. *Journal of Arthroplasty*, *29*(5), 955–960. https://doi.org/10.1016/j.arth.2013.10.020

Harrison, S. M., Whitton, R. C., Kawcak, C. E., Stover, S. M., and Pandy, M. G. (2010). Relationship between muscle forces, joint loading and utilization of elastic strain energy in equine locomotion. *Journal of Experimental Biology*, *213*(23), 3998–4009. https://doi.org/10.1242/jeb.044545

Hashemi, J., Chandrashekar, N., and Slauterbeck, J. (2005). The mechanical properties of the human patellar tendon are correlated to its mass density and are independent of sex. *Clinical Biomechanics*, *20*(6), 645–652. https://doi.org/10.1016/j.clinbiomech.2005.02.008

Haut, R. C., Lancaster, R. L., and DeCamp, C. E. (1992). Mechanical properties of the canine patellar tendon: Some correlations with age and the content of collagen. *Journal of Biomechanics*, *25*(2). https://doi.org/10.1016/0021-9290(92)90273-4

Hildreth, B. E., Marcellin-Little, D. J., Roe, S. C., and Harrysson, O. L. A. (2006). In vitro evaluation of five canine tibial plateau leveling methods. *American Journal of Veterinary Research*, *67*(4), 693–700. https://doi.org/10.2460/ajvr.67.4.693

Hosseini Nasab, S. H., Smith, C. R., Schütz, P., Postolka, B., List, R., and Taylor, W. R. (2019). Elongation Patterns of the Collateral Ligaments After Total Knee Arthroplasty Are Dominated by the Knee Flexion Angle. *Frontiers in Bioengineering and Biotechnology*, *7*(November), 1–12. https://doi.org/10.3389/fbioe.2019.00323

Hu, J., Chen, Z., Xin, H., Zhang, Q., and Jin, Z. (2018). Musculoskeletal multibody dynamics simulation of the contact mechanics and kinematics of a natural knee joint during a walking cycle. *Proceedings of the Institution of Mechanical Engineers, Part H: Journal of Engineering in Medicine*, *232*(5), 508–519. https://doi.org/10.1177/0954411918767695

Hunt, K. H., and Crossley, F. R. E. (1975). Coefficient of Restitution Interpreted as Damping in Vibroimpact. *Journal of Applied Mechanics*, *42*(2), 440–445. https://doi.org/10.1115/1.3423596

Johnson, A. L., Monsere, J., Sepulveda, G., Broaddus, K. D., Hauptman, J. G., and Marsh, S. (2006). Vertical Patellar Position in Large-Breed Dogs with Clinically Normal Stifles and Large-Breed Dogs with Medial Patellar Luxation. *Veterinary Surgery*, *35*(1), 78–81. https://doi.org/10.1111/j.1532-950x.2005.00115.x

Kang, K.-T., Koh, Y.-G., Jung, M., Nam, J.-H., Son, J., Lee, Y. H., Kim, S.-J., and Kim, S.-H. (2017). The effects of posterior cruciate ligament deficiency on posterolateral corner structures under gait- and squat-loading conditions. *Bone & Joint Research*, *6*(1), 31–42. https://doi.org/10.1302/2046-3758.61.bjr-2016-0184.r1

Kanno, N., Ochi, Y., Ichinohe, T., Hakozaki, T., Suzuki, S., Harada, Y., Yogo, T., and Hara, Y. (2019). Effect of the Centre of Rotation in Tibial Plateau Levelling Osteotomy on Quadriceps Tensile Force: An Ex Vivo Study in Canine Cadavers. *Veterinary and Comparative Orthopaedics and Traumatology*, *32*(02), 117–125. https://doi.org/10.1055/s-0039-1677868

Kebbach, M., Grawe, R., Geier, A., Winter, E., Bergschmidt, P., Kluess, D., D'Lima, D., Woernle, C., and Bader, R. (2019). Effect of surgical parameters on the biomechanical behaviour of bicondylar total knee endoprostheses – A robot-assisted test method based on a musculoskeletal

model. *Scientific Reports*, *9*(1), 14504. https://doi.org/10.1038/s41598-019-50399-3

Kim, H. Y., Kim, K. J., Yang, D. S., Jeung, S. W., Choi, H. G., and Choy, W. S. (2015). Screw-Home Movement of the Tibiofemoral Joint during Normal Gait: Three-Dimensional Analysis. *Clinics in Orthopedic Surgery*, *7*(3), 303. https://doi.org/10.4055/cios.2015.7.3.303

Kim, S. E., Pozzi, A., Banks, S. A., Conrad, B. P., and Lewis, D. D. (2009). Effect of tibial tuberosity advancement on femorotibial contact mechanics and stifle kinematics. *Veterinary Surgery*, *38*(1), 33–39. https://doi.org/10.1111/j.1532-950X.2008.00471.x

Kim, S. E., Pozzi, A., Banks, S. A., Conrad, B. P., and Lewis, D. D. (2010). Effect of cranial cruciate ligament deficiency, tibial plateau leveling osteotomy, and tibial tuberosity advancement on contact mechanics and alignment of the stifle in flexion. *Veterinary Surgery*, *39*(3), 363–370. https://doi.org/10.1111/j.1532-950X.2010.00655.x

Kim, S. E., Pozzi, A., Kowalesky, M. P., and Lewis, D. D. (2008). Tibial Osteotomies for Cranial Cruciate Ligament Insufficiency in Dogs. *Veterinary Surgery*, *37*(2), 111–125. https://doi.org/10.1111/j.1532-950X.2007.00361.x

Koh, Y., Jung, K., Hong, H., Kim, K., and Kang, K.-T. (2019). Optimal Design of Patient-Specific Total Knee Arthroplasty for Improvement in Wear Performance. *Journal of Clinical Medicine*, *8*(11), 2023. https://doi.org/10.3390/jcm8112023

Korvick, D. L., Pijanowski, G. J., and Schaeffer, D. J. (1994). Three-dimensional kinematics of the intact and cranial

cruciate ligament-deficient stifle of dogs. *Journal of Biomechanics*, *27*(1), 77–87. https://doi.org/10.1016/0021-9290(94)90034-5

Kweon, C., Lederman, E. S., and Chhabra, A. (2013). Anatomy and Biomechanics of the Cruciate Ligaments and Their Surgical Implications. In *The Multiple Ligament Injured Knee* (Vol. 9782287993, pp. 17–27). Springer New York. https://doi.org/10.1007/978-0-387-49289-6_2

Li, G., Gil, J., Kanamori, A., and Woo, S. L.-Y. (1999). A Validated Three-Dimensional Computational Model of a Human Knee Joint. *Journal of Biomechanical Engineering*, *121*(6), 657. https://doi.org/10.1115/1.2800871

Łojszczyk-Szczepaniak, A., Silmanowicz, P., Komsta, R., and Osiński, Z. (2017). Determination of reference values and frequency of occurrence of patella alta in German shepherd dogs: A retrospective study. *Acta Veterinaria Scandinavica*, *59*(1), 1–6. https://doi.org/10.1186/s13028-017-0304-1

Lopez, M. J., Hagquist, W., Jeffrey, S. L., Gilbertson, S., and Markel, M. D. (2004). Instrumented measurement of in vivo anterior-posterior translation in the canine knee to assess anterior cruciate integrity. *Journal of Orthopaedic Research*, *22*(5), 949–954. https://doi.org/10.1016/j.orthres.2003.10.017

Lopez, M. J., Kunz, D., Vanderby, R. J., Heisey, D., Bogdanske, J., and Markel, M. D. (2003). A comparison of joint stability between anterior cruciate intact and deficient knees: A new canine model of anterior cruciate ligament disruption. *Journal of Orthopaedic Research*, *21*(2), 224–230.

https://doi.org/10.1016/s0736-0266(02)00132-8

Mahadas, S., Mahadas, K., and Hung, G. K. (2019). Biomechanics of the golf swing using OpenSim. *Computers in Biology and Medicine*, *105*(December 2018), 39–45. https://doi.org/10.1016/j.compbiomed.2018.12.002

Manning, W., Ghosh, M., Wilson, I., Hide, G., Longstaff, L., and Deehan, D. (2019). Improved mediolateral load distribution without adverse laxity pattern in robot-assisted knee arthroplasty compared to a standard manual measured resection technique. *Knee Surgery, Sports Traumatology, Arthroscopy*, *0123456789*. https://doi.org/10.1007/s00167-019-05631-y

Marra, M. A., Vanheule, V., Fluit, R., Koopman, B. H. F. J. M., Rasmussen, J., Verdonschot, N., and Andersen, M. S. (2015). A Subject-Specific Musculoskeletal Modeling Framework to Predict In Vivo Mechanics of Total Knee Arthroplasty. *Journal of Biomechanical Engineering*, *137*(2), 020904. https://doi.org/10.1115/1.4029258

Mattern, K. L., Berry, C. R., Peck, J. N., and De Haan, J. J. (2006). Radiographic and ultrasonographic evaluation of the patellar ligament following tibial plateau leveling osteotomy. *Veterinary Radiology and Ultrasound*, *47*(2), 185–191. https://doi.org/10.1111/j.1740-8261.2006.00126.x

Milovancev, M., and Schaefer, S. (2009). Tibial Plateau Leveling Osteotomy. *Advances in Veterinary Surgery: The Canine Cranial Cruciate Ligament*, *02115*(1), 169–175.

Mizu-uchi, H., Colwell, C. W., Flores-Hernandez, C., Fregly, B. J., Matsuda, S., and D'Lima, D. D. (2015). Patient-Specific

Computer Model of Dynamic Squatting After Total Knee Arthroplasty. *The Journal of Arthroplasty*, *30*(5), 870–874. https://doi.org/10.1016/j.arth.2014.12.021

Morra, E. A., Rosca, M., Greenwald, J. F., and Greenwald, A. S. (2008). The Influence of Contemporary Knee Design on High Flexion: A Kinematic Comparison with the Normal Knee. *The Journal of Bone and Joint Surgery-American Volume*, *90*(Suppl 4), 195–201. https://doi.org/10.2106/JBJS.H.00817

Müller, J. H., Zakaria, T., van der Merwe, W., and D'Angelo, F. (2016). Computational modelling of mobile bearing TKA anterior–posterior dislocation. *Computer Methods in Biomechanics and Biomedical Engineering*, *19*(5), 549–562. https://doi.org/10.1080/10255842.2015.1045499

Navacchia, A., Rullkoetter, P. J., Schütz, P., List, R. B., Fitzpatrick, C. K., and Shelburne, K. B. (2016). Subject-specific modeling of muscle force and knee contact in total knee arthroplasty. *Journal of Orthopaedic Research*, *34*(9), 1576–1587. https://doi.org/10.1002/jor.23171

Nordin, M., and Frankel, V. H. (2012). Basic biomechanics of the musculoskeletal system. In *Basic Biomechanics of the Musculoskeletal System*. https://doi.org/10.1136/bjsm.26.1.69-a

Osmond, C. S., Marcellin-Little, D. J., Harrysson, O. L. A., and Kidd, L. B. (2006). Morphometric assessment of the proximal portion of the tibia in dogs with and without cranial cruciate ligament rupture. *Veterinary Radiology and Ultrasound*, *47*(2), 136–141. https://doi.org/10.1111/j.1740-

8261.2006.00119.x

Pascoletti, G., Cianetti, F., Putame, G., Terzini, M., and Zanetti, E. M. (2018). Numerical Simulation of an Intramedullary Elastic Nail: Expansion Phase and Load-Bearing Behavior. *Frontiers in Bioengineering and Biotechnology*, *6*(November), 1–11. https://doi.org/10.3389/fbioe.2018.00174

Pianigiani, S., Chevalier, Y., Labey, L., Pascale, V., and Innocenti, B. (2012). Tibio-femoral kinematics in different total knee arthroplasty designs during a loaded squat: A numerical sensitivity study. *Journal of Biomechanics*, *45*(13), 2315–2323. https://doi.org/10.1016/j.jbiomech.2012.06.014

Piazza, S. J., and Delp, S. L. (2001). Three-Dimensional Dynamic Simulation of Total Knee Replacement Motion During a Step-Up Task. *Journal of Biomechanical Engineering*, *123*(6), 599–606. https://doi.org/10.1115/1.1406950

Popescu, R., Haritinian, E. G., and Cristea, S. (2019). Relevance of Finite Element in Total Knee Arthroplasty - Literature Review. *Chirurgia*, *114*(4), 437. https://doi.org/10.21614/chirurgia.114.4.437

Pozzi, A., Kowaleski, M. P., Apelt, D., MEADOWS, C., ANDREWS, C. M., and JOHNSON, K. A. (2006). Effect of Medial Meniscal Release on Tibial Translation After Tibial Plateau Leveling Osteotomy. *Veterinary Surgery*, *35*(5), 486–494. https://doi.org/10.1111/j.1532-950X.2006.00180.x

Putame, G., Pascoletti, G., Franceschini, G., Dichio, G., and

Terzini, M. (2019). Prosthetic Hip ROM from Multibody Software Simulation. *2019 41st Annual International Conference of the IEEE Engineering in Medicine and Biology Society (EMBC)*, 5386–5389. https://doi.org/10.1109/EMBC.2019.8856993

Rahman, M., Cil, A., and Stylianou, A. (2018). Medial Collateral Ligament Deficiency of the Elbow Joint: A Computational Approach. *Bioengineering*, *5*(4), 84. https://doi.org/10.3390/bioengineering5040084

Rahman, M., Sharifi Renani, M., Cil, A., and Stylianou, A. (2018). Musculoskeletal Model Development of the Elbow Joint with an Experimental Evaluation. *Bioengineering*, *5*(2), 31. https://doi.org/10.3390/bioengineering5020031

Ramirez, J. M., Lefebvre, M., Böhme, B., Laurent, C., and Balligand, M. (2015). Preactivation of the quadriceps muscle could limit cranial tibial translation in a cranial cruciate ligament deficient canine stifle. *Research in Veterinary Science*, *98*, 115–120. https://doi.org/10.1016/j.rvsc.2014.11.012

Ranawat, A. S., and Ranawat, C. S. (2012). The history of total knee arthroplasty. In *The Knee Joint* (Vol. 33, Issue 1, pp. 699–707). Springer Paris. https://doi.org/10.1007/978-2-287-99353-4_63

Raske, M., Hulse, D., Beale, B., Saunders, W. B., Kishi, E., and Kunze, C. (2013). Stabilization of the CORA based leveling osteotomy for treatment of cranial cruciate ligament injury using a bone plate augmented with a headless compression screw. *Veterinary Surgery*, *42*(6), 759–764.

https://doi.org/10.1111/j.1532-950X.2013.12035.x

Renani, M. S., Rahman, M., Cil, A., and Stylianou, A. P. (2018). Calibrating multibody ulno-humeral joint cartilage using a validated finite element model. *Multibody System Dynamics*, *44*(1), 81–91. https://doi.org/10.1007/s11044-018-9622-y

Richard, J., Holler, P., Bockstahler, B., Dale, B., Mueller, M., Burston, J., Selfe, J., and Levine, D. (2010). A comparison of human and canine kinematics during level walking, Stair ascent, and Stair descent. *Wiener Tierarztliche Monatsschrift*, *97*(3–4), 92–100.

Sabatini, L., Risitano, S., Parisi, G., Tosto, F., Indelli, P. F., Atzori, F., and Massè, A. (2018). Medial Pivot in Total Knee Arthroplasty: Literature Review and Our First Experience. *Clinical Medicine Insights: Arthritis and Musculoskeletal Disorders*, *11*, 117954411775143. https://doi.org/10.1177/1179544117751431

Schiehlen, W. (1997). Multibody System Dynamics: Roots and Perspectives. *Multibody System Dynamics*, *1*(2), 149–188. https://doi.org/10.1023/A:1009745432698

Schindler, O. S., and Scott, W. N. (2011). Basic kinematics and biomechanics of the patello-femoral joint Part 1: The native patella. *Acta Orthopaedica Belgica*, *77*(4), 421–431.

Schmidt, R., Komistek, R. D., Blaha, J. D., Penenberg, B. L., and Maloney, W. J. (2003). Fluoroscopic Analyses of Cruciate-Retaining and Medial Pivot Knee Implants. *Clinical Orthopaedics and Related Research*, *410*(410), 139–147. https://doi.org/10.1097/01.blo.0000063565.90853.a4

Schünke, M., Schulte, E., Schumacher, U., Gaudio, E., Wesker,

K. H., and Voll, M. (2014). *Prometheus. Testo atlante di anatonomia. Anatomia generale e apparato locomotore*. Edises. https://books.google.it/books?id=IVHDoQEACAAJ

Seth, A., Hicks, J. L., Uchida, T. K., Habib, A., Dembia, C. L., Dunne, J. J., Ong, C. F., DeMers, M. S., Rajagopal, A., Millard, M., Hamner, S. R., Arnold, E. M., Yong, J. R., Lakshmikanth, S. K., Sherman, M. A., Ku, J. P., and Delp, S. L. (2018). OpenSim: Simulating musculoskeletal dynamics and neuromuscular control to study human and animal movement. *PLOS Computational Biology*, *14*(7), e1006223. https://doi.org/10.1371/journal.pcbi.1006223

Shelburne, K. B., and Pandy, M. G. (2002). A Dynamic Model of the Knee and Lower Limb for Simulating Rising Movements. *Computer Methods in Biomechanics and Biomedical Engineering*, *5*(2), 149–159. https://doi.org/10.1080/10255840290010265

Sherman, M. A., Seth, A., and Delp, S. L. (2011). Simbody: Multibody dynamics for biomedical research. *Procedia IUTAM*, *2*, 241–261. https://doi.org/10.1016/j.piutam.2011.04.023

Slocum, B., and Slocum, T. D. (1993). Tibial plateau leveling osteotomy for repair of cranial cruciate ligament rupture in the canine. *The Veterinary Clinics of North America. Small Animal Practice*, *23*(4), 777–795. https://doi.org/10.1016/S0195-5616(93)50082-7

Smith, C. R., Vignos, M. F., Lenhart, R. L., Kaiser, J., and Thelen, D. G. (2016). The Influence of Component Alignment and Ligament Properties on Tibiofemoral

Contact Forces in Total Knee Replacement. *Journal of Biomechanical Engineering*, *138*(2). https://doi.org/10.1115/1.4032464

Stylianou, A. P., Guess, T. M., and Kia, M. (2013). Multibody Muscle Driven Model of an Instrumented Prosthetic Knee During Squat and Toe Rise Motions. *Journal of Biomechanical Engineering*, *135*(4), 041008. https://doi.org/10.1115/1.4023982

Tanaka, Y., Nakamura, S., Kuriyama, S., Ito, H., Furu, M., Komistek, R. D., and Matsuda, S. (2016). How exactly can computer simulation predict the kinematics and contact status after TKA? Examination in individualized models. *Clinical Biomechanics*, *39*, 65–70. https://doi.org/10.1016/j.clinbiomech.2016.09.006

Tözeren, A. (2000). Human Body Dynamics. In *Human Body Dynamics*. Springer-Verlag. https://doi.org/10.1007/b97432

Trent, P. S., Walker, P. S., and Wolf, B. (1976). Ligament length patterns, strength, and rotational axes of the knee joint. *Clinical Orthopaedics and Related Research*, *117*, 263–270. https://doi.org/10.1097/00003086-197606000-00034

Twiggs, J. G., Wakelin, E. A., Roe, J. P., Dickison, D. M., Fritsch, B. A., Miles, B. P., and Ruys, A. J. (2018). Patient-Specific Simulated Dynamics After Total Knee Arthroplasty Correlate With Patient-Reported Outcomes. *The Journal of Arthroplasty*, *33*(9), 2843–2850. https://doi.org/10.1016/j.arth.2018.04.035

Verstraete, M. A., Meere, P. A., Salvadore, G., Victor, J., and Walker, P. S. (2017). Contact forces in the tibiofemoral joint

from soft tissue tensions: Implications to soft tissue balancing in total knee arthroplasty. *Journal of Biomechanics*, *58*, 195–202. https://doi.org/10.1016/j.jbiomech.2017.05.008

Viceconti, M., Ascani, D., and Mazzà, C. (2019). Pre-operative prediction of soft tissue balancing in knee arthoplasty part 1: Effect of surgical parameters during level walking. *Journal of Orthopaedic Research*, *37*(7), 1537–1545. https://doi.org/10.1002/jor.24289

Walker, P. S., Meere, P. A., and Bell, C. P. (2014). Effects of surgical variables in balancing of total knee replacements using an instrumented tibial trial. *The Knee*, *21*(1), 156–161. https://doi.org/10.1016/j.knee.2013.09.002

Warzee, C. C., Dejardin, L. M., Arnoczky, S. P., and Perry, R. L. (2001). Effect of tibial plateau leveling on cranial and caudal tibial thrusts in canine cranial cruciate-deficient stifles: An in vitro experimental study. *Veterinary Surgery*, *30*(3), 278–286. https://doi.org/10.1053/jvet.2001.21400

Wilke, V. L., Robinson, D. A., Evans, R. B., Rothschild, M. F., and Conzemius, M. G. (2005). Estimate of the annual economic impact of treatment of cranial cruciate ligament injury in dogs in the United States. *Journal of the American Veterinary Medical Association*, *227*(10), 1604–1607. https://doi.org/10.2460/javma.2005.227.1604

Wismans, J., Veldpaus, F., Janssen, J., Huson, A., and Struben, P. (1980). A three-dimensional mathematical model of the knee-joint. *Journal of Biomechanics*, *13*(8), 677–685. https://doi.org/10.1016/0021-9290(80)90354-1

Zanetti, E. M., Bignardi, C., Terzini, M., Putame, G., Alberto, L., and Bignardi, C. (2018). *A multibody model for the optimization of hip arthroplasty in relation to range of movement What this study adds : 11*(10), 486–491.

Zanetti, E., Terzini, M., Mossa, L., Bignardi, C., Costa, P., Audenino, A., and Vezzoni, A. (2017). A structural numerical model for the optimization of double pelvic osteotomy in the early treatment of canine hip dysplasia. *Veterinary and Comparative Orthopaedics and Traumatology*, *30*(04), 256–264. https://doi.org/10.3415/vcot-16-05-0065

Zapata, G., Sanz-Pena, I., Verstraete, M., and Walker, P. S. (2019). Effects of femoral component placement on the balancing of a total knee at surgery. *Journal of Biomechanics*, *86*(xxxx), 117–124. https://doi.org/10.1016/j.jbiomech.2019.01.056

Zaribaf, F. P. (2018). Medical-grade ultra-high molecular weight polyethylene: past, current and future. In *Materials Science and Technology (United Kingdom)* (Vol. 34, Issue 16, pp. 1940–1953). Taylor & Francis. https://doi.org/10.1080/02670836.2018.1469455

Zhang, Q., Chen, Z., Zhang, J., Hu, J., Peng, Y., Fan, X., and Jin, Z. (2019). Insert conformity variation affects kinematics and wear performance of total knee replacements. *Clinical Biomechanics*, *65*, 19–25. https://doi.org/10.1016/j.clinbiomech.2019.03.016

Zheng, G., and Nolte, L. P. (2015). Computer-Assisted Orthopedic Surgery: Current State and Future Perspective.

Frontiers in Surgery, *2*(December). https://doi.org/10.3389/fsurg.2015.00066

Ziegler, J. G., and Nichols, N. B. (1993). Optimum Settings for Automatic Controllers. *Journal of Dynamic Systems, Measurement, and Control*, *115*(2B), 220–222. https://doi.org/10.1115/1.2899060

Zumbrunn, T., Varadarajan, K. M., Rubash, H. E., Malchau, H., Li, G., and Muratoglu, O. K. (2015). Regaining Native Knee Kinematics Following Joint Arthroplasty: A Novel Biomimetic Design with ACL and PCL Preservation. *The Journal of Arthroplasty*, *30*(12), 2143–2148. https://doi.org/10.1016/j.arth.2015.06.017